Neutrino physics

Sin Kyu Kang
Seoul National University of Science and Technology, Seoul, Korea

In this lecture, I start with presenting the history of the neutrino from its invention to what we have discovered about its properties till now. I explain how we can observe neutrinos produced both naturally and artificially. Naturally produced neutrinos come to the Earth from the Sun, supernovae, collisions of cosmic rays with nuclei in the atmosphere, natural radioactivity, etc. On the other hand, those produced in accelerators and nuclear reactors are the examples of artificial neutrinos. I also illustrate what neutrino oscillations are and how such phenomena could be observed from various experiments to detect neutrinos produced in the aforementioned ways. Thanks to the discovery of neutrino oscillations, we are forced to modify the Standard Model, so as to accommodate the masses of neutrinos and lepton flavor mixing, which are essential to make neutrino flavor change. In fact, neutrinos can come in three different flavors, electron, muon and tau, and can change from one flavor to another. The origin of the tiny neutrino masses is still unknown, although we now know a few nice mechanisms capable of generating them. The generation of neutrino masses signifies physics beyond the Standard Model and can, therefore, be related to some of the unresolved fundamental issues, such as the origin of flavors, the unification of forces, the matter-antimatter asymmetry, etc. Some physicists believe that CP violation in neutrinos may be a missing piece in the understanding of the origin of the matter-antimatter asymmetry. I pedagogically explain how we can probe CP violation through neutrino oscillation experiments.

1 Introduction

1998 is the historic year in which neutrinos aroused great interest among not only physicists but also the public. The Super-Kamiokande (SK) Collaboration announced the first evidence of neutrino oscillations in that year [1]. This was the first experimental observation supporting the theory that the neutrino has non-zero mass, a possibility that theorists had speculated about for years. The discovery of neutrino oscillations was expected to bring fundamental changes to our knowledge of physics and astronomy. Though, many more discoveries about neutrinos have yet to be made.

1.1 Advent of neutrinos

Neutrinos were postulated by Pauli in 1930 to resolve the puzzle of the electron energy spectrum observed in beta decays, which show a continuous distribution instead of all electrons having the same energy. It seemed to contradict the principle of the conservation of energy. The puzzle can be solved if another unseen particle is emitted along with the electron in beta decay. Pauli originally called this particle the "neutron", but it was renamed the "neutrino" by Fermi in 1933. After the discovery of the neutron by Chadwick in 1932 [2], Fermi developed the theory of beta decay by proposing that four fermions directly interact with one another at one vertex [3]. By this interaction, the neutron decays directly to a proton, an electron and the proposed neutrino (what we now know to be an electron-antineutrino). The theory developed by Fermi, which proved to be successful, was the precursor to the theory of the weak

This article should be cited as: Neutrino physics, Sin Kyu Kang, DOI: 10.23730/CYRSP-2024-001.47, in: Proceedings of the 2022 Asia–Europe–Pacific School of High-Energy Physics,
CERN Yellow Reports: School Proceedings, CERN-2024-001, DOI: 10.23730/CYRSP-2024-001, p. 47.

interaction. Fermi first submitted his "tentative" theory of beta decay to the journal *Nature*, which rejected it "because it contained speculations too remote from reality to be of interest to the reader" [4]. Later, Nature admitted the rejection to be one of the great editorial blunders in its history.

1.2 Discovery of neutrinos

Neutrinos were first discovered by Reines and Cowan in 1956, who conducted the experiment to observe neutrinos through inverse beta decay ($\bar{\nu}_e + p \to n + e^+$) by using neutrinos from the Savannah River nuclear reactor [5]. In 1962, Lederman, Schwartz and Steinberger discovered a second neutrino by proving that the "muon" appeared to be accompanied by a neutrino that should be different from the neutrino appearing in beta decays [6]. The third generation charged lepton, called the "tau" lepton, has been discovered by Perl in 1975 [7]. As soon as the discovery of the tau lepton was announced, particle physicists speculated from experience that it would have a neutrino partner, the tau neutrino. It remained elusive until July 2000, when the DONUT experiment from Fermilab announced its discovery [8]. These three species of neutrinos are named electron-neutrino (ν_e), muon-neutrino (ν_μ) and tau-neutrino (ν_τ), associated to the charged leptons electron, muon and tau, respectively. Thanks to those experiments, the Standard Model (SM) of particle physics has been established to have six leptons consisting of three families, similarly to the quark sector.

1.3 Neutrinos in the Standard Model

In the SM, neutrinos are the only massless particles. There are exactly three neutrinos, one for each of the three charged leptons, as explained before and as confirmed by the observation of $e^+ + e^- \to Z^0 \to f\bar{f}$ at LEP experiments, with $N_\nu = \frac{\Gamma_{\rm inv}}{\Gamma_{\nu\bar{\nu}}} = 2.984 \pm 0.008$ [10]. All neutrinos are left-handed and all antineutrinos are right-handed in the SM. Since there are no right-handed (left-handed) neutrinos (antineutrinos), neutrinos have no mass. In the SM, neutrinos interact with matter only through weak interactions, which occur in two types, charged-current (CC) interactions and neutral-current (NC) interactions. The CC interactions occur through the exchange of a $W^\pm$, where the neutrino converts into the corresponding charged lepton (e.g. inverse beta decay, $\bar{\nu}_e + p \to n + e^+$). The NC interactions occur through the exchange of a Z^0, where the neutrino remains a neutrino, but transfers energy and momentum to whatever it interacted with.

2 Detection of neutrinos

2.1 Neutrino sources

Neutrinos are produced in the stars, the sky, nuclear reactors, human bodies, and even food like bananas. When we consider scientific research, there are several interesting sources that can help physicists study neutrinos: the sun, the atmosphere, reactors, accelerators, earth, the Big Bang, Supernovae, Extragalatic sources, etc. Huge numbers of neutrinos (about 10^{20} per second) are emitted in nuclear reactors, and also artificially produced in man-made accelerators delivering intense neutrino beams. But the main source of neutrinos is the Universe itself. The relic neutrinos from the Big Bang have been wandering for more than 13.6 billion years, with a density of 330 per cm^3 everywhere. Starting with the fusion of two protons, nuclear reactions in the core of the Sun produce about 2×10^{38} ν_e per second, which means

65 billions of neutrinos per second per cm^2 on Earth. Supernova explosions emit about 10^{58} neutrinos in a few seconds and the central engines of active galactic nuclei produce them abundantly.

2.2 How to detect neutrinos

Neutrinos rarely interact with ordinary matter, so they are very hard to detect. We can only detect the presence of a neutrino in our laboratory when it interacts through CC or NC interactions. Since a neutrino turns into its partner lepton via a CC interaction, the detection of a charged lepton is considered as a sign of a neutrino event. But, if the neutrino does not have sufficient energy to create its partner lepton, CC interaction is effectively unavailable to it. The neutrino enters and then leaves the detector after having transferred some of its energy and momentum to a target particle via NC interactions. The by-product created by the target particle hit by the neutrino is considered as a sign of a neutrino event. All three neutrinos can participate in NC interactions, regardless of the neutrino energy. In principle, CC interactions are easier to work with, because electrons and muons have characteristic signatures in particle detectors and are thus fairly easy to identify. They also have the advantage that they "flavor-tag" the neutrino. Various different detector technologies have been used in neutrino experiments over the years, depending on the requirements of the particular study. Among them, the following three are the most popular ones widely used.

- **Radiochemical experiments:** The lowest energy thresholds are provided by radiochemical experiments, in which the neutrino is captured by an atom which then (through inverse beta decay, a CC) converts into another element. The classic example is the chlorine solar neutrino experiment. Even lower thresholds were achieved by using gallium as the target: the reaction $^{71}\mathrm{Ga} + \nu \rightarrow {}^{71}\mathrm{Ge} + e^-$ has a threshold of only 0.233 MeV, and is even sensitive to pp neutrinos from the Sun. The produced isotope is unstable, and will decay back to the original element: neutrinos are counted by extracting the product and observing these decays. Examples of radiochemical experiments are Homestake (Ray Davis; chlorine); SAGE (gallium); GALLEX/GNO (gallium).
- **Liquid scintillator (LS) experiments:** LS has an impressive pedigree as neutrino detectors, since the neutrino was originally discovered using a LS detector. They are primarily sensitive to $\bar{\nu}_e$'s, which initiate inverse beta decay of a proton. Being organic compounds, LS is rich in hydrogen nuclei which act as targets for this reaction. The positron promptly annihilates, producing two gamma rays; the neutron is captured on a nucleus after a short time (a few microseconds to a few hundred microseconds), producing another gamma-ray signal. This coincidence of a prompt signal and a delayed signal allows the experiment to reject background effectively. LS detectors have good time and energy resolution, but do not preserve directional information. Examples of LS experiments are Borexino, KamLAND, MiniBooNE and SNO+.
- **Water Cherenkov experiments:** A particle travelling through a transparent medium at faster than the speed of light in that medium emits a kind of "light boom" – a coherent cone of blue light known as Cherenkov radiation. The particle is travelling down the axis of the cone, so if the cone can be reconstructed the direction of the particle can be measured. In a water Cherenkov detector, the Cherenkov radiation is detected, usually by photomultiplier tubes, and the cone of emission reconstructed. The axis of the cone gives the direction of the particle, and the light yield gives the

particle energy. Only charged particles with $\beta > 1/n$ can be detected, which gives a threshold total energy of about 0.8 MeV for electrons, 160 MeV for muons and 1.4 GeV for protons and neutrons. Neutrinos are detected in the detectors when they interact by W exchange, converting into muon or electron for ν_μ or ν_e respectively, or when they elastically scatter off electrons (when the recoil electron can be detected). Examples of densely instrumented water Cherenkov experiments are SK, far detector for the K2K and T2K experiments, and IMB.

3 Neutrino oscillation

3.1 History of neutrino oscillation

The idea of neutrino oscillation was first put forward in 1957 by Bruno Pontecorvo, who proposed that neutrino–antineutrino transitions may occur in analogy with neutral kaon mixing [11]. Although such a matter–antimatter oscillation had not been observed, this idea formed the conceptual foundation for the quantitative theory of neutrino flavor oscillation, which was first developed by Maki, Nakagawa, and Sakata (MNS) in 1962 [12] and further elaborated by Pontecorvo in 1967 [13], who developed the modern theory of neutrino oscillation in vacuum where the new ingredient is the mixing of different families of neutrinos introduced by MNS. One year later the solar neutrino deficit was first observed in Homestake in 1968 [14], and that was followed by the paper by Gribov and Pontecorvo published in 1969 [15]. Atmospheric neutrino experiments, IMB [17] and Kamiokande-II [18], found an anomaly in the ratio of the flux of muon to electron neutrinos. The SK reported the first evidence of the atmospheric neutrino oscillations in 1998 [1], and SNO experiments provided clear evidence of solar neutrino oscillations in 2001 [16]. Thanks to the discovery of neutrino oscillations, Kajita (SK) and McDonald (SNO) received the Nobel prize in 2015.

3.2 Neutrino mixing

To understand what neutrino oscillation is and how it occurs, we need to discriminate two kinds of neutrino quantum eigenstates: one is the flavor eigenstate and the other is the mass eigenstate. Flavor eigenstates, denoted by $(\nu_e, \nu_\mu, \nu_\tau)$, are the quantum states produced or detected via weak interactions together with charged leptons with the same flavor (e, μ, τ). Mass eigenstates, denoted by (ν_1, ν_2, ν_3), are the states of definite masses that are created by the interactions with Higgs boson or other mechanisms. The mismatch between flavor states and mass states of neutrinos gives rise to neutrino mixing. Then, a specific flavor state of a neutrino is given by a superposition of three mass eigenstates having definite masses, written as

$$\nu_l = \sum_{i=1}^{N} U_{li}\nu_i \quad , \tag{1}$$

where $l = e, \mu, \tau$ and $i = 1, 2, 3$, and U_{li} denotes a 3×3 unitary matrix, the so-called Pontecorvo–Maki–Nakagawa–Sakita mixing matrix. The neutrino mixing elements mean how much each flavor can contribute to the composition of each mass states, and how much each flavor is accompanied by a certain mass eigenstate in the weak interaction. The 3×3 unitary mixing matrix is generally represented by 3 mixing angles and 6 phases. However, not all phases are physical observables. Let us see how many

phases are physical by assuming neutrinos are Dirac particles. Under global phase transformations of the leptons, neutrinos (ν_k) and charged leptons (l_α) are transformed as $\nu_k \to e^{i\varphi_k}\nu_k$ ($k = 1, 2, 3$) and $l_\alpha \to e^{i\varphi_\alpha} l_\alpha$ ($\alpha = e, \mu, \tau$). Then, the terms of the Lagrangian for the CC interactions in the mass basis, $\mathcal{L}_{cc} = \frac{g}{\sqrt{2}}\overline{\nu}_k U^\dagger \gamma^\mu l_\alpha W^+_\mu$, become

$$\sum_{k=1}^{3}\sum_{\alpha=e,\mu,\tau} \overline{\nu}_{kL} e^{-i\varphi_k} U^*_{\alpha k} e^{i\varphi_\alpha}\gamma^\rho l_{\alpha L} \Rightarrow e^{-i(\varphi_1-\varphi_e)}\sum_{k=1}^{3}\sum_{\alpha=e,\mu,\tau} \overline{\nu}_{kL} e^{-i(\varphi_k-\varphi_1)} U^*_{\alpha k} e^{i(\varphi_\alpha-\varphi_e)}\gamma^\rho l_{\alpha L} \quad . \tag{2}$$

In the right-handed side of Eq. (2), 5 phases can be eliminated by redefining lepton fields. Finally, we see that the 3×3 unitary mixing matrix can be expressed in terms of 3 mixing angles and 1 phase. In the standard parameterization, the lepton mixing matrix can be expressed as

$$\begin{aligned} U &= \begin{pmatrix} 1 & 0 & 0 \\ 0 & c_{23} & s_{23} \\ 0 & -s_{23} & c_{23} \end{pmatrix} \begin{pmatrix} c_{13} & 0 & s_{13}e^{-i\delta} \\ 0 & 1 & 0 \\ -s_{13}e^{i\delta} & 0 & c_{13} \end{pmatrix} \begin{pmatrix} c_{12} & s_{12} & 0 \\ -s_{12} & c_{12} & 0 \\ 0 & 0 & 1 \end{pmatrix} \\ &= \begin{pmatrix} c_{12}c_{13} & s_{12}c_{13} & s_{13}e^{-i\delta_{\rm CP}} \\ -s_{12}c_{23} - c_{12}s_{23}s_{13}e^{i\delta_{\rm CP}} & c_{12}c_{23} - s_{12}s_{23}s_{13}e^{i\delta_{\rm CP}} & s_{23}c_{13} \\ s_{12}s_{23} - c_{12}c_{23}s_{13}e^{i\delta_{\rm CP}} & -c_{12}s_{23} - s_{12}c_{23}s_{13}e^{i\delta_{\rm CP}} & c_{23}c_{13} \end{pmatrix} \quad , \end{aligned} \tag{3}$$

where c_{ij} and s_{ij} denote $\cos\theta_{ij}$ and $\sin\theta_{ij}$, respectively, and $\delta_{\rm CP}$ is a Dirac CP violating phase. If neutrinos are Majorana particles, then there exist two extra CP violating phases. As will be shown later, the mixing angles θ_{23}, θ_{12} and θ_{13} are associated with oscillations of atmospheric neutrinos, solar neutrinos and reactor neutrinos, respectively.

3.3 Neutrino oscillations in vacuum

Neutrino oscillations are quantum mechanical phenomena where flavor and mass eigenstates mismatch. Then, flavor eigenstates of neutrinos are superpositions of mass eigenstates, written as $|\nu_\alpha\rangle = \sum_k U_{\alpha k}|\nu_k\rangle$ with $\alpha = (e, \mu, \tau), k = (1, 2, 3)$. The time evolution of flavor eigenstates is given by

$$\begin{aligned} |\nu_\alpha(t,x)\rangle &= \sum_k U_{\alpha k} e^{-i(E_k t + p_k x)}|\nu_k\rangle = \sum_\beta \left(\sum_k U_{\alpha k} e^{-i(E_k t + p_k x)} U^*_{\beta k}\right)|\nu_\beta\rangle \\ &= \sum_\beta \mathcal{A}_{\nu_\alpha\to\nu_\beta}(t,x)|\nu_\beta\rangle \quad , \end{aligned} \tag{4}$$

where $\mathcal{A}_{\nu_\alpha\to\nu_\beta}(t,x)$ denotes the amplitude of the neutrino flavor transition and E_k, p_k are neutrino energy and momentum. From Eq. (4), one can easily obtain the probability of the neutrino flavor transition,

$$P_{\nu_\alpha\to\nu_\beta}(t,x) = \left|\mathcal{A}_{\nu_\alpha\to\nu_\beta}(t,x)\right|^2 = \left|\sum_k U_{\alpha k} e^{-i(E_k t + p_k x)} U^*_{\beta k}\right|^2 . \tag{5}$$

In natural units, $t = x$, we can make an approximation as follows:

$$E_k t - p_k x \simeq (E_k - p_k)L = \frac{E_k^2 - p_k^2}{E_k + p_k} L = \frac{m_k^2}{E_k + p_k} L \simeq \frac{m_k^2}{2E} L \quad , \tag{6}$$

where L is the distance of neutrino propagation. Then, the probability is given by

$$P_{\nu_\alpha \to \nu_\beta}(t, x) = \left| \sum_k U_{\alpha k} e^{-i m_k^2 L/2E} U_{\beta k}^* \right|^2 = \sum_{k,j} U_{\alpha k} U_{\beta k}^* U_{\alpha j} U_{\beta j}^* \mathrm{Exp}\left(-i \frac{\Delta m_{kj}^2 L}{2E} \right) \quad , \tag{7}$$

where $\Delta m_{kj}^2 \equiv m_k^2 - m_j^2$.

As an example, let us consider the two-flavor oscillation with ν_e and ν_μ, for which the states produced and detected are supposedly $|\nu_\mu\rangle = -\sin\theta|\nu_1\rangle + \cos\theta|\nu_2\rangle$ and $|\nu_e\rangle = \cos\theta|\nu_1\rangle + \sin\theta|\nu_2\rangle$, respectively. For this case, the transition (appearance) probability is given by

$$P_{\nu_\mu \to \nu_e}(L, E) = 2\sin^2\theta\cos^2\theta \left(1 - \cos\left(\frac{\Delta m_{21}^2 L}{2E} \right) \right) = \sin^2 2\theta \sin^2\left(\frac{\Delta m_{21}^2 L}{4E} \right) . \tag{8}$$

In the above expression, there are two fundamental parameters, θ and Δm_{21}^2, which are determined from neutrino oscillation experiments for given L and E. The neutrino oscillation length is defined by $L^{\mathrm{osc}} \equiv \frac{4\pi E}{\Delta m^2}$. The so-called survival (disappearance) probability is given by

$$P_{\nu_\mu \to \nu_\mu}(L, E) = 1 - P_{\nu_\mu \to \nu_e}(L, E) = 1 - \sin^2 2\theta \sin^2\left(\frac{\Delta m_{21}^2 L}{4E} \right) . \tag{9}$$

Figure 1 shows how the transition probability evolves along with L/E. The maximum height of the

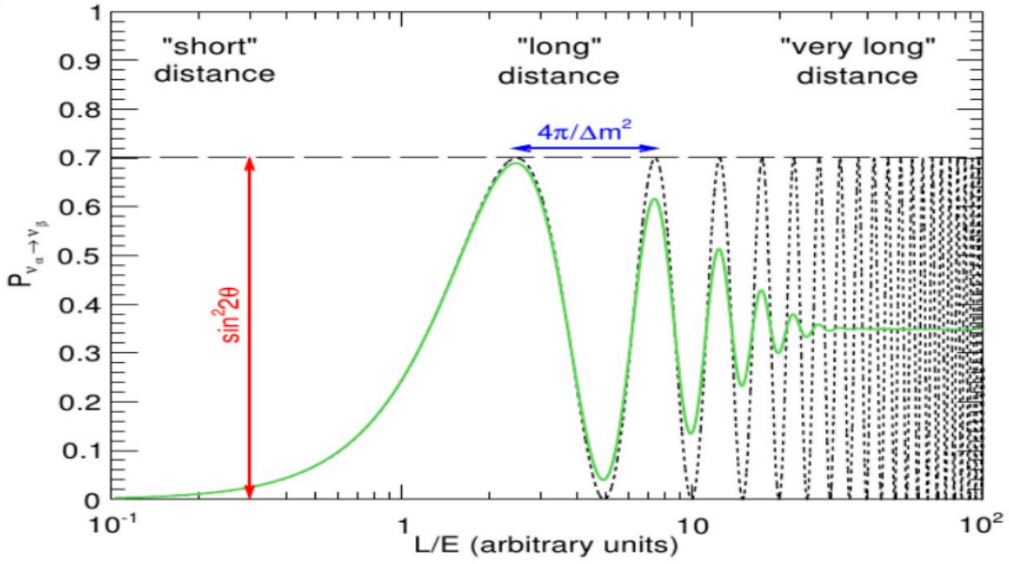

Fig. 1: Plot of the transition probability $P_{\nu_\alpha \to \nu_\beta}(L, E)$ in terms of L/E (figure taken from Ref. [19]).

curve corresponds to $\sin^2 2\theta$, and the horizontal distance between the first and second peak is $4\pi/\Delta m^2$. At very long distances, it is averaged out to be half of the maximum height.

Extending to the three-flavor paradigm, the probability of neutrino oscillation is given explicitly by

$$\begin{aligned} P_{\nu_\alpha\to\nu_\beta} = \quad & \underbrace{\delta_{\alpha\beta} - 4\sum_{i<j}^{3} \mathrm{Re}(U_{\alpha i}U_{\beta i}U^*_{\alpha j}U^*_{\beta j}) \sin^2\left(\frac{\Delta m^2_{ji}L}{2E}\right)}_{\text{CP conserving part: } = P^{\rm CPC}_{\nu_\alpha\to\nu_\beta}} \\ + \quad & \underbrace{2\sum_{i<j}^{3} \mathrm{Im}(U_{\alpha i}U_{\beta i}U^*_{\alpha j}U^*_{\beta j}) \sin\left(\frac{\Delta m^2_{ji}L}{2E}\right)}_{\text{CP violating part : } = P^{\rm CPV}_{\nu_\alpha\to\nu_\beta}} \quad , \end{aligned} \tag{10}$$

where the first two terms correspond to the CP conserving part ($\equiv P^{\rm CPC}_{\nu_\alpha\to\nu_\beta}$), whereas the last one to the CP violating part ($\equiv P^{\rm CPV}_{\nu_\alpha\to\nu_\beta} = 8J\sum_\gamma \epsilon_{\alpha\beta\gamma} \sin\frac{\Delta m^2_{21}L}{4E} \sin\frac{\Delta m^2_{31}L}{4E} \sin\frac{\Delta m^2_{32}L}{4E}$). In the limit that $\Delta m^2_{21} = \Delta m^2_{\rm sol} \ll |\Delta m^2_{\rm atm}| = |\Delta m^2_{31}| \simeq |\Delta m^2_{32}|$, the survival and transition probabilities are approximately given by

$$\begin{aligned} P_{\nu_\alpha\to\nu_\alpha} &\simeq 1 - 4|U_{\alpha1}|^2|U_{\alpha2}|^2 \sin^2\left(\frac{\Delta m^2_{21}L}{4E}\right) - 4(1-|U_{\alpha3}|^2)|U_{\alpha3}|^2 \sin^2\left(\frac{\Delta m^2_{31}L}{4E}\right) \ , \\ P_{\nu_\alpha\to\nu_\beta} &\simeq -4(U_{\alpha1}U_{\beta1}U^*_{\alpha2}U^*_{\beta2}) \sin^2\left(\frac{\Delta m^2_{21}L}{4E}\right) + 4|U_{\alpha3}|^2|U_{\beta3}|^2 \sin^2\left(\frac{\Delta m^2_{31}L}{4E}\right) \ . \end{aligned} \tag{11}$$

In addition, since the mixing angle θ_{13} is small compared with the two others, $|U_{e3}|^2 \ll |U_{e1}|^2, |U_{e2}|^2$, and $U_{e1} \simeq \cos\theta_{12}, U_{e2} \simeq \sin\theta_{12}$. Adopting those approximations, the electron neutrino survival probability is simply given by

$$P_{\nu_e\to\nu_e} \simeq 1 - \sin^2 2\theta_{12} \sin^2\left(\frac{\Delta m^2_{21}L}{4E}\right) . \tag{12}$$

This result shows that the effect of solar neutrino oscillations is decoupled from that of atmospheric neutrino oscillations. So, the formula (12) is good at probing solar neutrinos. On the other hand, in the case that we can ignore the oscillating terms involving Δm^2_{21}, the oscillation probabilities are given by

$$\begin{aligned} P_{\nu_\alpha\to\nu_\alpha} &\simeq 1 - 4(1-|U_{\alpha3}|^2)|U_{\alpha3}|^2 \sin^2\left(\frac{\Delta m^2_{31}L}{4E}\right) \ , \\ P_{\nu_\alpha\to\nu_\beta} &\simeq 4|U_{\alpha3}|^2|U_{\beta3}|^2 \sin^2\left(\frac{\Delta m^2_{31}L}{4E}\right) \ . \end{aligned} \tag{13}$$

These expressions are relevant to the atmospheric and short baseline reactor neutrino experiments.

3.4 Neutrino oscillations in matter

Wolfenstein for the first time studied a matter effect that may convert the flavor of a neutrino into another one [20]. When neutrinos pass through matter, they experience forward scattering, mostly from electrons they encounter along the way, which represents a contribution to the Hamiltonian with a potential proportional to the density of electrons in matter. Similarly to optics, the net effect of this coherent elastic scattering is the appearance of a phase difference, a refractive index, or equivalently, a neutrino effective mass. As a result, the oscillation probability can be rather different from that in vacuum. For the case of

the two-flavor scenario, the 2×2 Hamiltonian in matter is given by

$$\mathcal{H}_M = \mathcal{H}_{\rm vac} + \begin{pmatrix} V_e & 0 \\ 0 & V_\mu \end{pmatrix} = \begin{pmatrix} V & 0 \\ 0 & 0 \end{pmatrix} + \lambda'' I \ , \tag{14}$$

where $V_{\alpha(=e,\mu)}$ denotes the potential energy associated with ν_α and the term proportional to the unit matrix I is irrelevant for flavor evolution. V is defined by $V_e - V_\mu = \sqrt{2} G_F N_e$, where G_F and N_e are the Fermi constant and electron number density in matter, respectively. $\mathcal{H}_{\rm vac}$ is given by

$$\mathcal{H}_{\rm vac} = \frac{\Delta m^2}{4E} \begin{pmatrix} -\cos 2\theta & \sin 2\theta \\ \sin 2\theta & \cos 2\theta \end{pmatrix} \ , \tag{15}$$

where we have used $p \simeq E$, with E being the average energy of the neutrinos. If N_e is constant, diagonalizing $\mathcal{H}_M$ leads us to modifications of the mixing angle and of the mass-squared difference, denoted by θ_M and Δm^2_M, respectively. The explicit forms of θ_M and Δm^2_M are given as

$$\begin{aligned} \tan 2\theta_M &= \frac{\tan 2\theta}{1 - \frac{A_{CC}}{\Delta m^2 \cos 2\theta}} \ , \\ \Delta m^2_M &= \sqrt{(\Delta m^2 \cos 2\theta - A_{CC})^2 + (\Delta m^2 \sin 2\theta)^2} \ , \end{aligned} \tag{16}$$

where $A_{CC} = 2\sqrt{2} G_F N_e E$ and $(\theta, \Delta m^2)$ are the parameters in vacuum. Such a modification of the parameters in matter leads to a shift of the mass eigenstates, which are related to flavor eigenstates as follows:

$$\begin{aligned} |\nu_e\rangle &= \cos\theta_M |\nu_{1m}\rangle + \sin\theta_M |\nu_{2m}\rangle \ , \\ |\nu_\mu\rangle &= -\sin\theta_M |\nu_{1m}\rangle + \cos\theta_M |\nu_{2m}\rangle \ , \end{aligned} \tag{17}$$

where $|\nu_{im}\rangle$ denotes the mass eigenstate in matter. Mikheyev and Smirnov found that when $A_{CC} = \Delta m^2 \cos 2\theta$, resonance occurs and neutrino mixing becomes maximal, with $\theta_M = \pi/4$ [21]. In a medium with constant density, there is no transition between ν_{1m} and ν_{2m}, which are the eigenstates of propagation, so oscillation probability is simply given by $P_{\nu_e \to \nu_\mu} \simeq \sin^2 2\theta_M \sin\left(\frac{\Delta m^2_M L}{4E}\right)$, which is similar to the probability in vacuum.

In case that matter density varies with time, it is hard to solve the time-dependent Schrödinger equations for neutrinos analytically. In this case, ν_{1m} and ν_{2m} are not propagation eigenstates any longer and transition between them occurs. Let us suppose that ν_e is produced in matter and detected later in vacuum. Then, the flavor eigenstates in the production and detection are given by

$$\begin{aligned} \text{production} : \quad |\nu_e\rangle &= \cos\theta_M |\nu_{1m}\rangle + \sin\theta_M |\nu_{2m}\rangle \ , \\ \text{detection} : \quad |\nu_e(x)\rangle &= \cos\theta |\nu_1(x)\rangle + \sin\theta |\nu_2(x)\rangle \ . \end{aligned} \tag{18}$$

Neglecting the interference term, the average survival (appearance) probability is given by [22]

$$\bar{P}_{\nu_e \to \nu_\mu}(x) = \frac{1}{2} + \left(\frac{1}{2} - P_c\right) \cos 2\theta_M \cos 2\theta \ , \tag{19}$$

where P_c represents the transition probability between ν_{1m} and ν_{2m}. An interesting limit exists, which is called "adiabatic limit", where the time evolution of the neutrino state is sufficiently slow, and then each state evolves independently and transitions between ν_{1m} and ν_{2m} can be neglected. In the adiabatic limit, $P_c = 0$ and then the probability $\bar{P}_{\nu_e \to \nu_\mu}$ becomes

$$\bar{P}_{\nu_e \to \nu_\mu}(x) \;=\; \cos^2\theta \cos^2\theta_M + \sin^2\theta \sin^2\theta_M \;. \tag{20}$$

There are two interesting limits. In the limit that $\Delta m^2/2E \ll \sqrt{2} G_F N_e$, θ_M goes to $\pi/2$ and then the probability becomes $\bar{P}_{\nu_e \to \nu_\mu} \simeq \sin^2\theta$. In the limit that $\Delta m^2/2E \gg \sqrt{2} G_F N_e$, θ_M goes to the vacuum angle and then the probability becomes $\bar{P}_{\nu_e \to \nu_\mu} \simeq 1 - \frac{1}{2}\sin^2 2\theta$. These results are useful to interpret the flux deficits of solar neutrinos observed at various experiments, as will be discussed later.

4 Neutrino experiments

4.1 Atmospheric neutrino experiments

Neutrino oscillation was discovered for the first time through the studies of atmospheric neutrinos, which are produced by cosmic-ray interactions with nuclei in the atmosphere. Electron-neutrinos and muon-neutrinos are produced mainly by the decay chain of charged pions to muons and to electrons. The event ratio of ν_μ to ν_e, $R_{\mu/e} = (N_{\nu_\mu} + N_{\bar{\nu}_\mu})/(N_{\nu_e} + N_{\bar{\nu}_e})$, is expected to be nearly 2 below about 1 GeV, based on the calculations of neutrino fluxes produced from interactions in the atmosphere, as shown in Ref. [23]. Above this energy, the ratio increases due to the increasing probability of muons reaching the ground before their decay. So, whether the ratio remains 2 in the detection of atmospheric neutrinos or not is a good indicator for neutrino oscillation. In early-stage experiments such as Soudan 2 [24], IMB [17] and Kamiokande [18], a deficit of $R_{\mu/e}$ was observed, but it was unclear whether this was due to neutrino oscillations or not. Another important hint toward the understanding of the atmospheric neutrino flux deficit was given in Ref. [25]. The atmospheric neutrinos enter the spherical Earth at a point

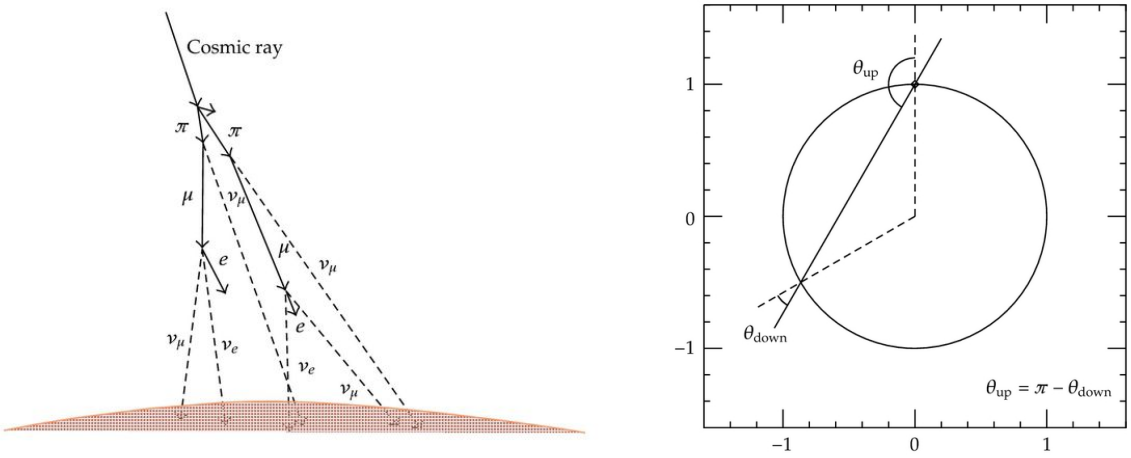

Fig. 2: Schematic figure of the production of atmospheric neutrinos (left) and a neutrino trajectory that enters a spherical Earth with a zenith angle $\theta_{\rm down}$ and exits with $\theta_{\rm up}$ (right). These figures are taken from Ref. [26].

with a zenith angle $\theta_{\rm down}$ and should exit the Earth at a point with $\theta_{\rm up}$. Obviously, $\theta_{\rm down}$ and $\theta_{\rm up}$ are related by $\theta_{\rm down} = \pi - \theta_{\rm up}$, as can be seen in Fig. 2. Since cosmic rays enter into the atmosphere with approximately equal rate in every position in the Earth, the numbers of downward-going and upward-going neutrinos must be the same. Thus the flux is expected to be up-down symmetric. The Kamiokande data [18] showed that the deficit of μ-like events depended on the zenith angle, but with relatively poor event statistics.

In 1996, a much larger detector, SK, started taking data. The SK experiment used a 50 kt water Cherenkov detector, and has obtained data with substantially improved statistics in 1998. The events observed in SK are classified by 4 types. Events where vertex positions are located inside the fiducial volume of the detector and all visible secondary particles stop in the detector are called "fully-contained" (FC) events. The "partially-contained" (PC) events are ν_μ events with multi-GeV neutrino energies, producing energetic muons which do not stop in the detector. High-energy ν_μ interactions in the rock below the detector produce high-energy muons, which enter into the detector. Some of them stop in the detector and are called "upward stopping muons", others penetrate through the detector and are called "upward through-going muons". Figure 3 shows several plots of zenith angle dependence for the results

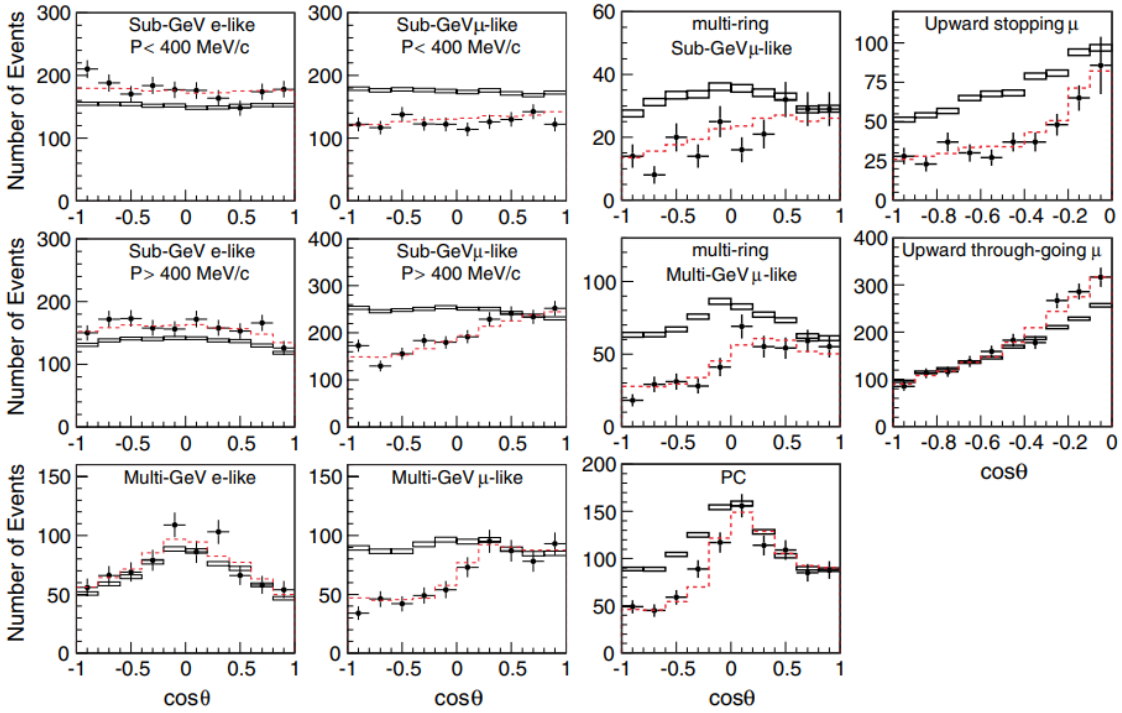

Fig. 3: Zenith angle distributions of μ- and e-like events at sub-GeV and multi-GeV scales from the SK 92 kt·year data for various data samples [26]. $\cos\theta = 1(-1)$ corresponds to down(up)-going. The solid-line histograms show the prediction without neutrino oscillations. The dashed-line histograms show the prediction with oscillation ($\nu_\mu \to \nu_\tau$) for $\Delta m^2_{32} = 2.1 \times 10^{-3}$ eV^2 and $\sin^2 2\theta_{23} = 1.0$.

obtained by SK [26]. From the results, we see that the deficit of upward-going μ-like events depends on the zenith angle in the multi-GeV energy range, the ν_μ to ν_e event ratio is smaller than what was expected, the ratio of upward-going stopping/through-going muons is smaller than what was expected,

and the zenith angle distribution for the upward through-going muons is distorted. These results represent an evidence of the neutrino oscillation for which muon-neutrinos convert to other flavors of neutrinos through their flight inside the Earth.

According to the neutrino oscillation formulae, the neutrino survival probability should follow the sinusoidal function. The ν_μ survival probability should have a minimum at a certain L/E value, come back to unity after traveling twice the distance, and continue oscillating. Using high L/E resolution events only, SK found that the ν_μ survival probability shows a dip at a position corresponding to the first minimum of the survival probability. Figure 4 shows the updated plot based on the 220 kt·yrs data of

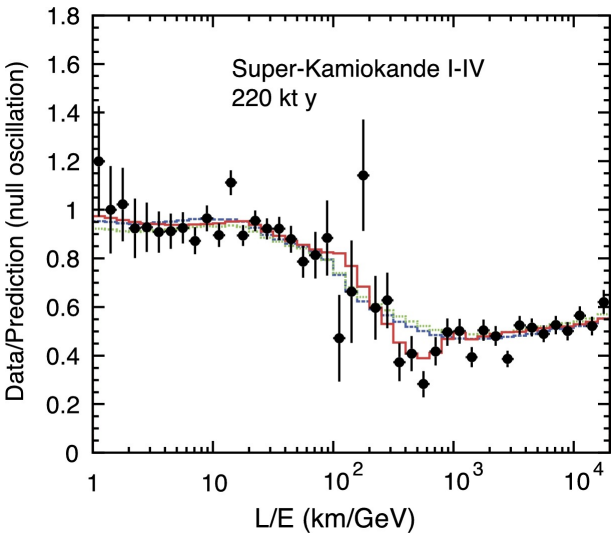

Fig. 4: The ratio of data to MC events without oscillation as a function of the reconstructed L/E, together with the best-fit 3-flavor expectation for neutrino oscillation and two alternative hypotheses with similar shape. The dashed (blue) and dotted (green) lines show the best-fit expectations for neutrino decay and neutrino decoherence, respectively. Figure taken from Ref. [27].

SK-I through SK-IV [27]. This was the first evidence that the ν_μ survival probability is represented by a sinusoidal function as predicted by neutrino oscillations. In Fig. 4, the expected ν_μ survival probabilities by neutrino oscillations as well as those from alternative models, which were able to explain the zenith angle distributions, are shown with the detector L/E resolution taken into account. It is clear that the alternative models cannot reproduce the dip seen near $L/E = 500$ km/GeV. Thanks to this result, alternative hypotheses for the atmospheric neutrino flux deficit, such as neutrino decay (blue dashed) and neutrino decoherence (green dotted), are ruled out.

Figure 5 shows the allowed regions of neutrino oscillation parameters (Δm^2, $\sin^2 2\theta$) at 68% (dashed curves) and 90% (solid curves) C.L. from several experiments [27]. The thick-black and thick-gray curves represent the allowed regions based, respectively, on the zenith angle analysis and the L/E analyses in SK. Results from K2K (thin-gray) and MINOS (thin-black) experiments are plotted. The mixing angle is consistent with the maximum mixing ($\sin^2 2\theta = 1.0$). These parameters are much more accurately measured compared with those in 1998.

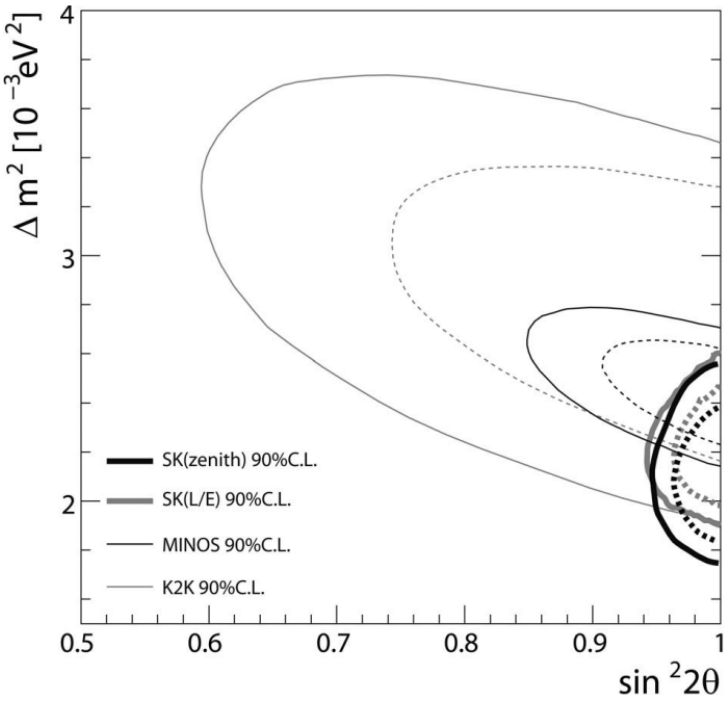

Fig. 5: Allowed regions of (Δm^2 and $\sin^2 2\theta$) at 68 (dashed lines) and 90% (solid lines) C.L. from various experiments (figure taken from Ref. [27]). Thick-black and thick-gray lines show the allowed regions based on the zenith-angle analysis and L/E analyses in SK, respectively. Also shown are the allowed regions from K2K (thin-gray lines) and MINOS (thin-black lines) experiments.

4.2 Accelerator based neutrino experiments

One of the ways physicists can study neutrinos effectively is by making intense neutrino beams using proton accelerators. The neutrinos produced in accelerators are typically muon neutrinos, and the machine can be tuned to create either neutrinos or antineutrinos. Figure 6 represents an overview of the neutrino beam production from NuMI (Neutrinos at Main Injector), which is used at Fermilab to create an intense beam of neutrinos aimed toward detectors in experiments such as MINOS, MINERνA, NOνA etc. Accelerator neutrinos are used to study neutrino interactions and neutrino oscillations taking advan-

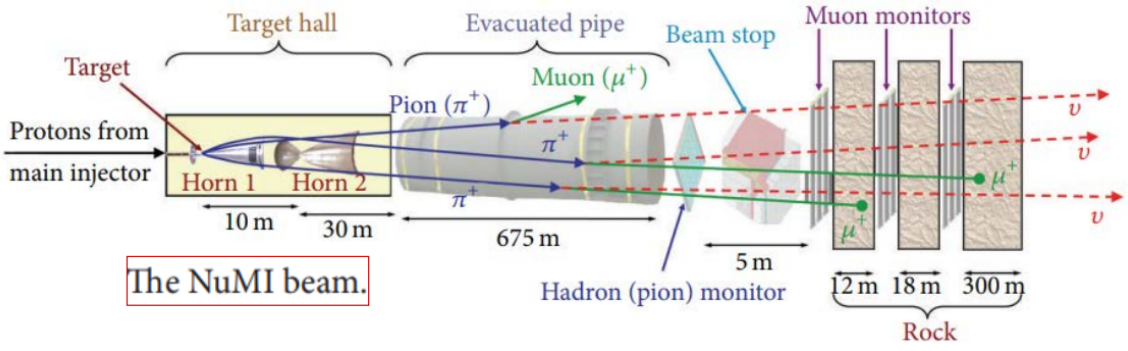

Fig. 6: Overview of neutrino beam production from NuMI [28].

tage of high-intensity neutrino beams, as well as a possibility of controlling and understanding their type and kinematic properties to a much larger extent than for neutrinos from other sources. Neutrino beams can be used for two different kinds of experiments, distinguished by how far away the detectors are from where the neutrinos are made: short baseline (SBL) and long baseline (LBL) experiments. In the case of SBL experiments using accelerator neutrinos, the detector sits close to the neutrino source, so that the beam is very concentrated when it reaches the detector. The experiments are good for characterizing the beam and learning about the neutrinos before they oscillate, and are also a good place to hunt for sterile neutrinos and see how neutrinos interact with other particles. In the case of LBL experiments, they focus on the oscillations while traveling a long distance through the Earth. Neutrinos have many opportunities to interact with matter and have sufficient distance to change flavors. They are a good place to figure out mass ordering (MO) and CP violation in the neutrino sector.

The off-axis neutrino beam results in a narrow band energy distribution of the produced neutrinos, due to the correlation between the off-axis angle and neutrino energy [29]. The accelerator neutrino beam is primarily a wide beam that has no clear boundaries, because the neutrinos in it do not move in parallel, but have a certain angular distribution. The further away from the axis of the beam, the smaller the number of neutrinos, and the distribution of energy also changes. The energy spectrum becomes narrower and its maximum moves to lower energy. The off-axis angle can be optimized to maximize the neutrino oscillation probability or to select an energy range in which the desired type of neutrino interaction is dominant.

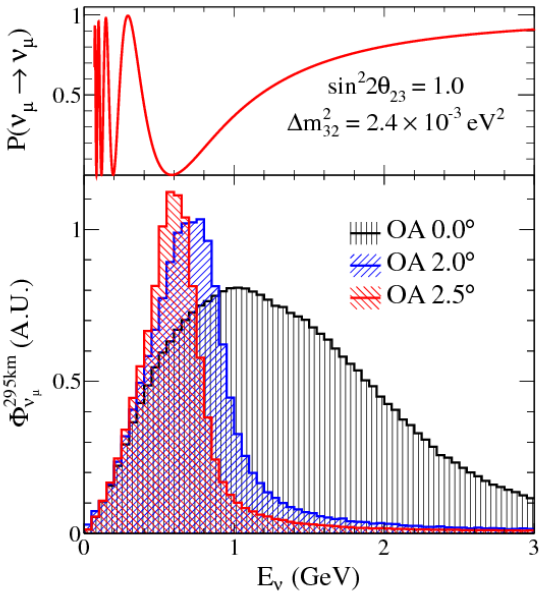

Fig. 7: ν_μ survival probability at 295 km (up) and ν_μ flux (down) versus E_ν at T2K. Back, blue and red regions correspond to the flux for axis angles of $0°, 2.0°, 2.5°$, respectively [32].

The first experiment with an off-axis neutrino beam was the T2K experiment, a LBL experiment located in Japan [30]. The main components of T2K include a neutrino beam line, muon monitors, a near detector complex ND280 located at 280 m from the proton interaction target, and the far detector of SK (295 km from the neutrino source), at a 2.5 degree off-axis angle from the beam. The physics goals

of T2K are (1) to improve the measurement of Δm^2_{32} and $\sin^2\theta_{23}$ using the ν_μ disappearance analysis, and (2) to measure for the first time the θ_{13} oscillation parameter through the ν_e appearance analysis. As illustrated in the lower panel of Fig. 7, the peak energy of the neutrino beam varies with different off-axis angles. For T2K, the off-axis angle is at 2.5°, so that the neutrino beam at SK has a peak energy at about 0.6 GeV, close to the expected first oscillation maximum [32]. In 2011, T2K first announced the observation of ν_e appearance events in a ν_μ beam [31]. It also provided the world's best measurement of the oscillation parameter θ_{23} and the first hint of CP violation in neutrino oscillations.

The MINOS experiment is designed to study the phenomena of neutrino oscillations by making precision neutrino oscillation measurements using the neutrino beam produced by NuMI [33]. Neutrinos are observed in two detectors, one very close to where the beam is produced (near detector), and another much larger detector 735 km away from northern Minnesota (far detector). MINOS measures the difference in neutrino beam composition and energy distribution in both detectors for the purpose of precision measurements of Δm^2_{23} and θ_{23}. In addition, MINOS looks for the appearance of ν_e in the far detector, and will either measure or set a limit on the oscillation probability of ν_μ into ν_e. By observing the disappearance of ν_μ, MINOS has made the world's most precise measurement of the larger neutrino mass splitting and has measured θ_{23} [34]. Using a dedicated antineutrino beam, MINOS has also made the first direct precision measurements of the corresponding antineutrino parameters [34]. A search for ν_e and $\bar{\nu}_e$ appearance has enabled a measurement of the mixing angle θ_{13}. MINOS has performed the first search for $\bar{\nu}_e$ appearance in a ν_μ beam and the first search for ν_e and $\bar{\nu}_e$ appearance with significant matter effects. MINOS will continue as MINOS+ [35] using an upgraded beam with higher energy and intensity, allowing precision tests of the three-flavour neutrino oscillation picture, in particular a very sensitive search for the existence of sterile neutrinos.

The NOνA experiment [36] is designed to mainly observe the oscillation of ν_μ to ν_e by using the NuMI beam and consists of two detectors, one in Fermilab and the other in northern Minnesota, allowing neutrinos to travel more than 810 km. It is also capable of measuring $\delta_{\rm CP}$ through the comparison between the $\nu_\mu \to \nu_e$ and $\bar{\nu}_\mu \to \bar{\nu}_e$ oscillation channels. Recently, NOνA [37] provided a less precise measurement of $\delta_{\rm CP}$, which is in slight tension with the T2K result (as will be shown later). Figure 8 shows the allowed regions of oscillation parameters $(\Delta m^2_{32}, \sin^2\theta_{23})$ at 90% C.L. We note that the contours overlap. NOνA, T2K and IceCube prefer the upper octant of θ_{23}, while SK prefers the lower one.

4.3 Solar neutrino experiments

Solar neutrinos are produced by nuclear fusion in the Sun's core and are the most common type of neutrinos passing through any source observed on Earth. The vast majority of neutrinos are produced through the pp chain, a process in which four protons are combined to produce two protons, two neutrons, two positrons, and two electron neutrinos, but their energy is so low (< 0.425 MeV) [13] that they are very difficult to detect [39]. The electron capture of ^{7}Be produces neutrinos at either roughly 0.862 MeV ($\sim 90\%$) or 0.384 MeV ($\sim 10\%$). A rare side branch of the pp chain produces the ^{8}B neutrinos with a maximum energy of roughly 15 MeV, and these are the easiest neutrinos to detect [39]. A very rare interaction in the pp chain produces the "hep" neutrinos, the highest energy neutrinos (up to 18 MeV) predicted to be produced by the Sun [39]. Neutrinos are also produced by the CNO cycle, but that process

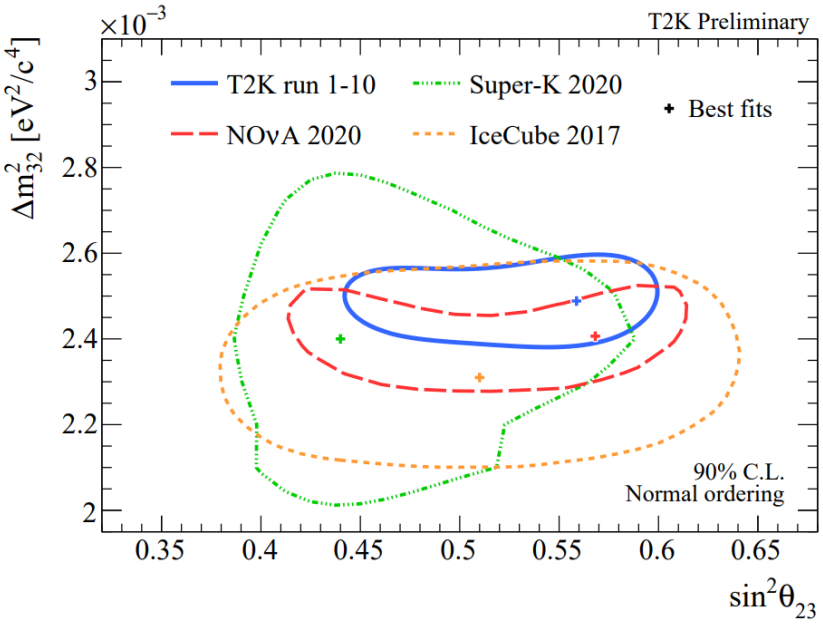

Fig. 8: Allowed regions of (Δm^2_{32}, $\sin^2\theta_{23}$) at 90% C.L. from various experiments (figure taken from Ref. [38]).

is considerably less important in the Sun than in other stars [39].

The timeline of solar neutrinos and their discovery dates back to the 1960s, beginning with the two astrophysicists John N. Bahcall and Raymond Davis Jr. The experiment, known as the Homestake experiment, aimed to count the solar neutrinos arriving on Earth. Using the standard solar model (SSM), Bahcall was able to calculate the number of neutrinos arriving on Earth from the Sun [40]. At the same time, Davis had proposed an idea to detect solar neutrinos by using a radioactive chemical process: $\nu_e + {}^{37}\mathrm{Cl} \rightarrow {}^{37}\mathrm{Ar} + e^-$ [41]. By conducting the experiment deep underground, they were able to avoid cosmic ray interactions which could affect the process and results. As a surprise, the experimental value of observed solar neutrinos was less than 20% of the theoretical prediction calculated by Bahcall [14]. It was unknown at the time whether there were errors in the experiment or calculations, or whether Bahcall and Davis did not explain all variables, but this discrepancy gave birth to what became known as the solar neutrino problem. Later, the deficits of the solar neutrino flux were observed in some other experiments such as GALLEX [42], SAGE [43] and SK [44], with numbers ranging from one half to two thirds. One year after the discovery of neutrino oscillation at SK, the Sudbury Neutrino Observatory (SNO) started collecting data [45]. That experiment aimed at observing the ${}^8\mathrm{B}$ solar neutrinos with around 10 MeV energy, and was designed to employ a large quantity of heavy water as the detection medium, which could make it possible to observe both the electron neutrinos produced in the core of the Sun and all flavors of neutrinos. The experiment was able to observe two separate reactions on deuteron, a CC reaction that was sensitive only to ν_e and a NC that was equally sensitive to all flavors. Also, SNO could observe neutrinos of all flavors via the elastic scattering (ES) of electrons by neutrinos. The neutrino flux in each

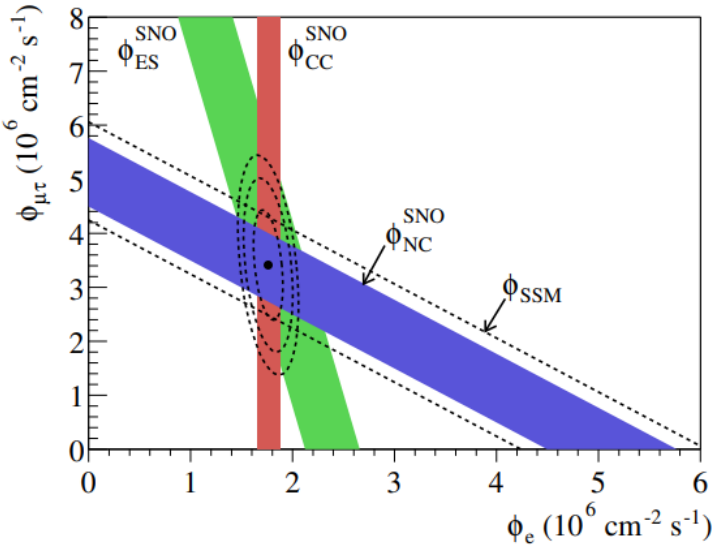

Fig. 9: Flux of ^{8}B solar neutrinos from SNO, measured via CC, NC and ES interactions. The axes represent the inferred fluxes of $\nu_\mu + \nu_\tau$ and ν_e. The sensitivity to NC and ES interactions give the slopes of the bands. The solar neutrino flux predicted by the SSM [49] is indicated as $\phi_{\rm SSM}$ (dashed line). The intercepts of these bands with the axes represent the $\pm 1\sigma$ errors. The dashed ellipses represent the best estimates of $\phi(\nu_e)$ and $\phi(\nu_{\mu\tau})$ at $1\sigma, 2\sigma$ and 3σ C.L.

reaction is parameterized in terms of the flux of each flavor as follows [46]:

$$\begin{aligned} \phi_{CC} &= \phi(\nu_e)\ , \\ \phi_{ES} &= \phi(\nu_e) + 0.1559\ \phi(\nu_{\mu\tau})\ , \\ \phi_{CC} &= \phi(\nu_e) + \phi(\nu_{\mu,\tau})\ , \end{aligned} \tag{21}$$

where $\phi(\nu_{\mu\tau}) = \phi(\nu_\mu) + \phi(\nu_\tau)$ and the factor of 0.1559 is the ratio of the ES cross sections for $\nu_{\mu\tau}$ and ν_e above $T_{\rm eff} = 5.0$ MeV. Making this change of variables and fitting directly for the flavor content, the null hypothesis test of no-oscillation is reduced to a test of the condition $\phi(\nu_{\mu\tau}) = 0$. With the measurements of the systematic uncertainties on both acceptance and detector response, the results of the flux for the constrained fit are given in units of 10^6 cm^{-2}s^{-1} by [47]

$$\begin{aligned} \phi_{CC} &= 1.76^{+0.06}_{-0.05}({\rm stat})^{+0.09}_{-0.09}({\rm syst})\ , \\ \phi_{ES} &= 2.39^{+0.24}_{-0.23}({\rm stat})^{+0.12}_{-0.12}({\rm syst})\ , \\ \phi_{NC} &= 5.09^{+0.44}_{-0.43}({\rm stat})^{+0.46}_{-0.43}({\rm syst})\ . \end{aligned} \tag{22}$$

The physical interpretation of the "flux" for each interaction type is that it is the equivalent flux of ^{8}B ν_e's produced from an undistorted energy spectrum that would yield the same number of events inside the signal region from that interaction as was seen in the data. It turns out that about 1/3 of solar ν_e survived while 2/3 are transformed into the combined ν_μ and ν_τ. The inequality of the fluxes determined from the CC, ES, and NC reactions strongly supported the evidence for the existence of non-ν_e components to the ^{8}B solar neutrinos. Figure 9 shows the constraints on the ν_e flux $\phi(\nu_e)$ versus the combined ν_μ and

ν_τ fluxes $\phi(\nu_{\mu\tau})$, derived from the CC, ES, and NC rates. Both measurements of the total active fluxes ϕ_{NC}, as well as the sum of $\phi(\nu_e) + \phi(\nu_{\mu\tau})$, were in good agreement with SSM predictions, which could confirm the validity of the SSM predictions on the solar neutrino fluxes.

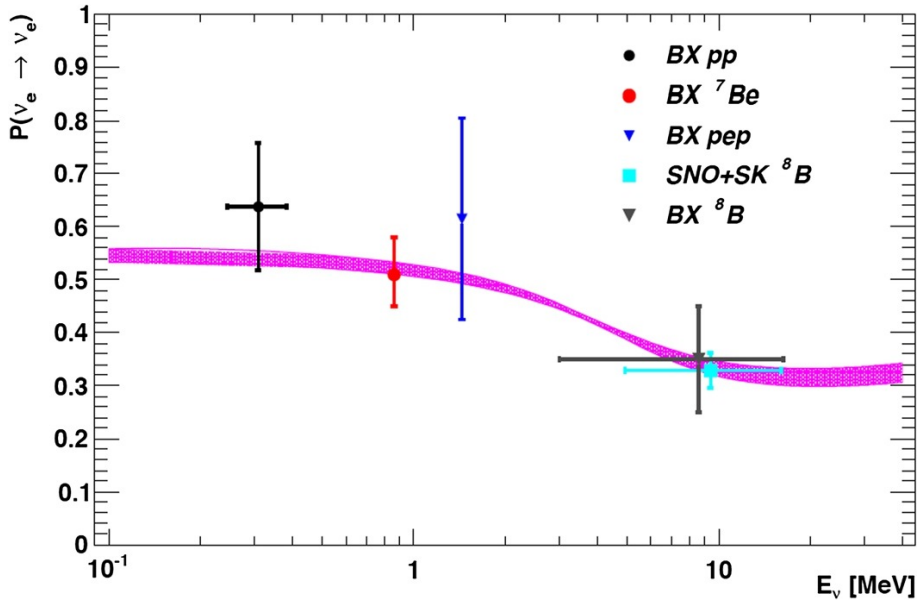

Fig. 10: Measurements of the ν_e survival probability, obtained by Borexino, as well as SNO and SK (figure taken from Ref. [51]). The shaded regions represent the MSW-LMA predictions.

The phenomenon of solar neutrino transition is complicated by the matter effect, as neutrinos propagate outwards from their production point inside the Sun. As discussed before, the so-called "MSW" effect, proposed by Mikheyev, Smirnov and Wolfenstein, enhances oscillation in an energy-dependent fashion. As a result, neutrinos produced in different fusion reactions are affected to a different extent, due to their different energies. While the MSW effect is negligible at sub-MeV energies, where vacuum oscillation dominates, it becomes significant above about 5 MeV. The former case is relevant for the results from the gallium experiments such as GALLEX and SAGE, which were sensitive to low energy *pp* neutrinos, resulting in $\bar{P}_{\nu_e \to \nu_\mu} \simeq 1 - \frac{1}{2}\sin^2 2\theta \simeq 0.6$. The latter condition is assumed to explain the results from SK and SNO, which mostly detected ^{8}B neutrinos, resulting in $\bar{P}_{\nu_e \to \nu_\mu} \simeq \sin^2\theta \simeq 0.32$. A transition is predicted in between these two regimes, where the survival probability falls from the vacuum-averaged value to the additionally-suppressed matter oscillation value. It is worthwhile to note that in both the vacuum- and matter-dominated regions the survival probability is determined by the value of the mixing angle, θ_{12}, and not by the details of the interaction of neutrinos with matter.

In 2011, the Borexino experiment [50] first confirmed the energy dependence of the oscillation probability as well as the transition between two regimes for solar neutrinos, as presented in Fig. 10, which is taken from Ref. [51].

4.4 Reactor based neutrino experiments

4.4.1 KamLAND experiment

This was the first experiment aiming to find evidence for neutrino oscillation using a terrestrial source of $\overline{\nu}_e$ produced from nuclear reactors in Japan. KamLAND detected hundreds of $\overline{\nu}_e$ through the inverse beta decay $\overline{\nu}_e + p \to n + e^+$ with a $\overline{\nu}_e$ energy threshold of 1.8 MeV, achieving an enormous improvement over previous attempts from any other detectors. The 180 km baseline, together with the emitted $\overline{\nu}_e$ spectrum, made KamLAND sensitive to neutrino oscillation with large mixing angle (LMA) as a solution to the solar neutrino problem. Figure 11 shows the ratio of the measured to the expected flux for KamLAND, as well as for previous reactor experiments, as a function of the average distance from the source. The solid red circle corresponds to the KamLAND result obtained at a flux weighted average distance of 180 km. The shaded region indicates the range of flux predictions corresponding to the 95% C.L. LMA region from a global analysis of the solar neutrino data. Earlier measurements have seen no trace of anomaly, whereas the first data from KamLAND [52] give a lower ratio, exactly as expected by the LMA solution to the solar neutrino problem. The dotted curve, drawn with $\sin^2 2\theta = 0.833$ and $\Delta m^2 = 5.5 \times 10^{-5}\,\mathrm{eV}^2$, is representative of a best-fit LMA prediction. The L_0/E distribution plotted in Fig. 12 shows the oscillatory behavior of the KamLAND data [53]. The solid (blue), dash (red) and dash-dot (green) histograms are the expectations from the best-fit oscillations, best-fit decay and best-fit decoherence, taking into account the individual time-dependent flux variations of all reactors and detector effects. It turns out that the data from KamLAND follow the oscillatory shape of reactor $\overline{\nu}_e$'s arising from the neutrino oscillation.

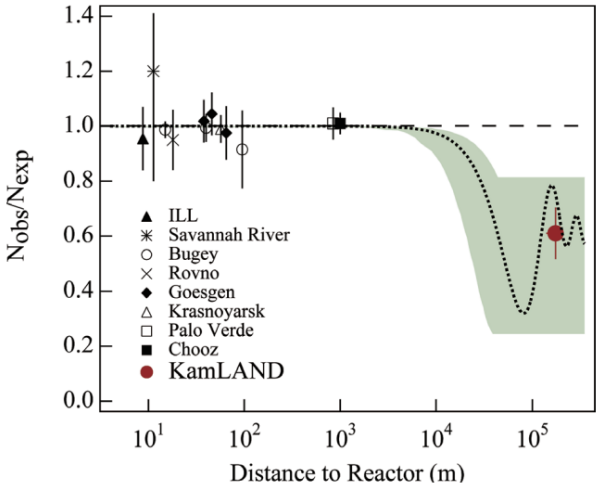

Fig. 11: The ratio of measured to expected $\bar{\nu}_e$ flux for reactor experiments (figure taken from Ref. [52]).

Compatibility of KamLAND with solar neutrino experiments: Figure 13 presents the allowed region of parameter space $(\Delta m^2_{21}, \sin^2\theta_{12})$ from solar neutrino experiments (green region) and from KamLAND (blue region). The two results are compatible at the 1.1σ level, and the tension between solar global result and KamLAND data is significantly reduced compared with the old data from solar neutrinos. Combining both results, we obtain the region in red.

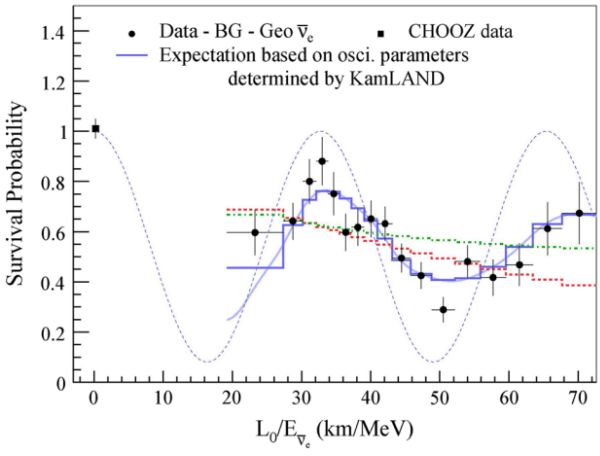

Fig. 12: Ratio of the background- and geoneutrino-subtracted $\bar{\nu}_e$ spectrum to the expectation for no-oscillation, as a function of $L_0(=180\text{km})/E$ [53]. The solid (blue), dashed (red) and dot-dashed (green) histograms are the expectations from the best-fit oscillations, best-fit decay and best-fit decoherence.

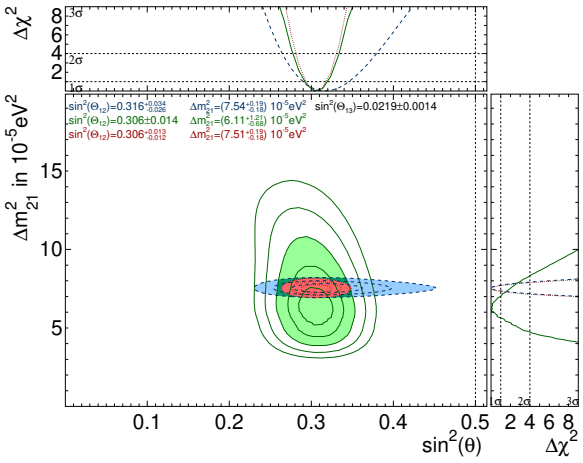

Fig. 13: Allowed regions of parameter space $(\Delta m^2_{21}, \sin^2\theta_{12})$ from solar neutrino experiments (green contours and green region) and from KamLAND (blue region) (figure taken from Ref. [54]). The red region is the combined result. The filled regions give the 3σ C.L. results, the other contours shown are at the 1 and 2σ C.L.

4.4.2 Measuring θ_{13}

The mixing angle θ_{13} is a key parameter to understand the underlying structure of neutrino mixing as well as to explore whether CP is violated in the lepton sector. There are lots of different ways to learn about θ_{13}. Two of the most popular involve particle accelerators and nuclear reactors. The best measurements of θ_{13} come from nuclear reactor experiments such as Double Chooz [55], RENO [56] and Daya Bay [57]. Detectors located near nuclear reactors provide such wonderful readings of θ_{13}

because reactors produce an extremely pure fountain of $\bar{\nu}_e$'s, and θ_{13} is closely tied to how ν_e's mix. Reactor experiments look for the disappearance of $\bar{\nu}_e$ in the flux from the operating fission reactors. This provides an intense source of neutrinos, in the energy range of a few MeV. The signal channel is the inverse beta decay reaction on protons. The coincidence signal from the prompt positron and the delayed neutron capture allows the unique identification of $\bar{\nu}_e$ events. For neutrinos in this energy range we can ignore Earth's matter effect and the survival probability is quite simply given by

$$P_{\bar{\nu}_e \to \bar{\nu}_e} \simeq 1 - \sin^2 2\theta_{13} \sin^2 \frac{\Delta m^2_{31} L}{4E} - \cos^4 \theta_{13} \sin^2 2\theta_{12} \sin^2 \frac{\Delta m^2_{21} L}{4E} \,. \tag{23}$$

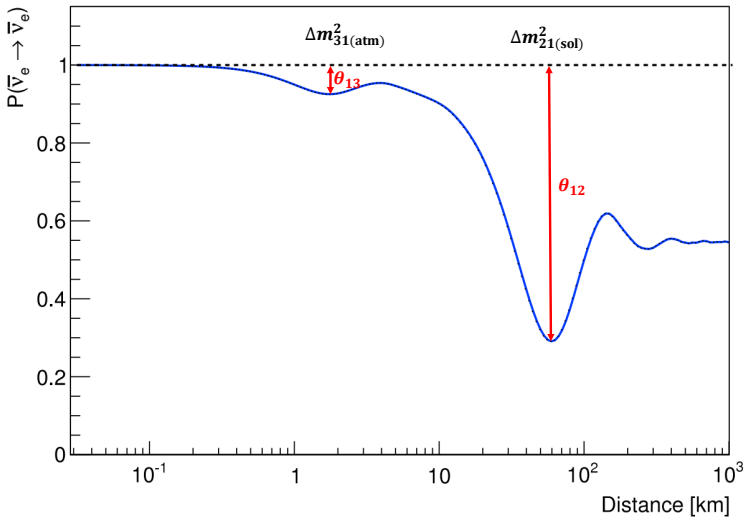

Fig. 14: $P_{\bar{\nu}_e \to \bar{\nu}_e}$ in terms of L for short baseline ($L = 1$–2 km) and medium baseline($L \sim 60$ km) reactor neutrinos.

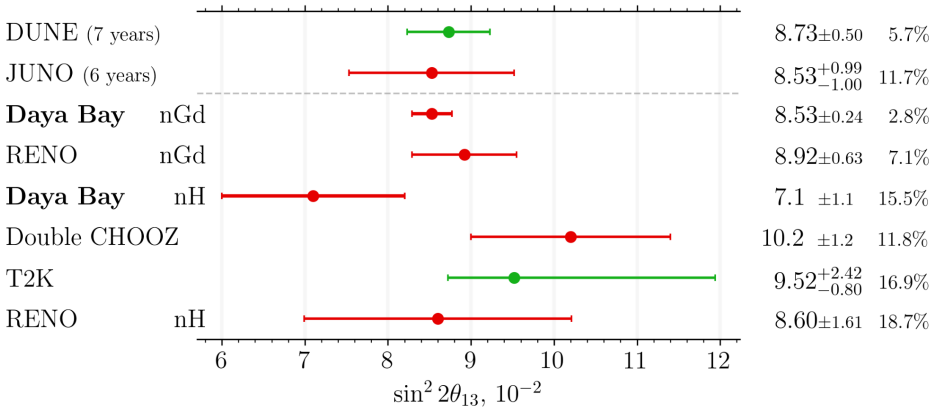

Fig. 15: Comparison of the recent published results for θ_{13} from Daya Bay, RENO, Double Chooz, and T2K, as well as the expected sensitivities of future experiments released by Daya Bay.

Figure 14 shows how $P_{\bar{\nu}_e \to \bar{\nu}_e}$ evolves with L for short baseline and medium baseline neutrinos. On a 1–2 km baseline, the third (solar scale) term is around 1% of the second (atmospheric scale) term, so

it contributes very little uncertainty to the probability. As a result the survival probability gives direct access to $\sin^2 2\theta_{13}$. Unlike the LBL experiments, the measurement of θ_{13} through the reactor experiment is theoretically clean but, by the same token, they cannot determine the MO or find CP violation. On the other hand, the third term is dominant over the second one for about 60 km baseline, such as for the JUNO experiment [58]. Based on clear deficits of $\overline{\nu}_e$ fluxes compared with the no-oscillation predictions as well as the energy dependence of the oscillation probability, Daya Bay, RENO and Double Chooz have measured the values of θ_{13} in 2012 [59–61], which turned out to be surprisingly large. Figure 15 presents the comparison of the recent published results for θ_{13} from Daya Bay, RENO, Double Chooz and T2K, as well as the expected sensitivities of future experiments released by Daya Bay.

4.5 Global fit to neutrino data

Three-flavor oscillation parameters from the global fit to data as of November 2022 are presented in Fig. 16 [62]. The results shown in the upper (lower) section are obtained without (with) the inclusion of the tabulated χ^2 data on atmospheric neutrinos provided by SK (SK-atm). The numbers in the 1st and 2nd column are obtained by assuming the neutrino mass spectrum to be normal ordering (NO) and inverted ordering (IO), respectively. The minimization with respect to IO provides the same results as NO, except for the 3σ range of Δm^2_{3l} in the analysis without SK-atm. Note that $\Delta m^2_{3l} = \Delta m^2_{31} > 0$ for NO and $\Delta m^2_{3l} = \Delta m^2_{32} < 0$ for IO. Figure 17 shows the results of the χ^2 analysis for the 3-flavor oscillation [62]. The red (blue) curves are for NO (IO). The solid (dashed) lines are obtained without (with) the inclusion of SK-atm χ^2 data. For atmospheric Δm^2, we use Δm^2_{31} for NO and Δm^2_{32} for IO. From the results, we see that $\theta_{13}, \theta_{12}, \Delta m^2_{21}, |\Delta m^2_{31}|$ are well-measured, whereas the MO, the octant of θ_{23} and CP phase have yet to be determined.

5 Neutrino mass

Neutrinos were presumed to be massless. Despite decades of experimental efforts, the only evidence we have that neutrino masses are not zero comes from neutrino oscillation experiments. The masses of neutrinos are still a mystery. It is a fundamental and important question, "how much mass do neutrinos have?". Measuring their masses would help point toward new physics beyond the SM. What we know from the neutrino oscillation experiments are the two square-mass differences $\Delta m^2_{21} \sim 7.5 \times 1^{-5}$ eV^2 and $|\Delta m^2_{31}| \sim 2.5 \times 10^{-3}$ eV^2. A recent combination of Planck data with Type Ia supernova luminosity distances, Baryon Acoustic Oscillcation (BAO), and determinations of the growth rate parameter set the most constraining bound to date, $\sum_i m_i < 0.12$ eV at 95% C.L. [63], which is based on the assumption of the Λ (cosmological constant) cold dark matter model of the Big Bang theory. Although such constraint from cosmic surveys is indirect, it is safe to say that all three neutrino masses are smaller than 1 eV.

5.1 Neutrino mass ordering

Since the sign of the atmospheric mass splitting ($|\Delta m^2_{31}| \sim 2 \times 10^{-3}$ eV^2) remains unknown, there are two options for the neutrino MO: *normal* and *inverted*. On the other hand, since Δm^2_{21} turned out to be positive from the solar neutrino experiments considering the matter effect, ν_2 is always assumed to be heavier than ν_1. In the NO (IO), ν_3 is the heaviest (lightest) neutrino. Figure 18 shows the pictorial

NuFIT 5.2 (2022)

		Normal Ordering (best fit)		Inverted Ordering ($\Delta\chi^2 = 2.3$)	
		bfp $\pm 1\sigma$	3σ range	bfp $\pm 1\sigma$	3σ range
without SK atmospheric data	$\sin^2\theta_{12}$	$0.303^{+0.012}_{-0.011}$	$0.270 \to 0.341$	$0.303^{+0.012}_{-0.011}$	$0.270 \to 0.341$
	$\theta_{12}/^\circ$	$33.41^{+0.75}_{-0.72}$	$31.31 \to 35.74$	$33.41^{+0.75}_{-0.72}$	$31.31 \to 35.74$
	$\sin^2\theta_{23}$	$0.572^{+0.018}_{-0.023}$	$0.406 \to 0.620$	$0.578^{+0.016}_{-0.021}$	$0.412 \to 0.623$
	$\theta_{23}/^\circ$	$49.1^{+1.0}_{-1.3}$	$39.6 \to 51.9$	$49.5^{+0.9}_{-1.2}$	$39.9 \to 52.1$
	$\sin^2\theta_{13}$	$0.02203^{+0.00056}_{-0.00059}$	$0.02029 \to 0.02391$	$0.02219^{+0.00060}_{-0.00057}$	$0.02047 \to 0.02396$
	$\theta_{13}/^\circ$	$8.54^{+0.11}_{-0.12}$	$8.19 \to 8.89$	$8.57^{+0.12}_{-0.11}$	$8.23 \to 8.90$
	$\delta_{\rm CP}/^\circ$	197^{+42}_{-25}	$108 \to 404$	286^{+27}_{-32}	$192 \to 360$
	$\frac{\Delta m^2_{21}}{10^{-5}\ {\rm eV}^2}$	$7.41^{+0.21}_{-0.20}$	$6.82 \to 8.03$	$7.41^{+0.21}_{-0.20}$	$6.82 \to 8.03$
	$\frac{\Delta m^2_{3\ell}}{10^{-3}\ {\rm eV}^2}$	$+2.511^{+0.028}_{-0.027}$	$+2.428 \to +2.597$	$-2.498^{+0.032}_{-0.025}$	$-2.581 \to -2.408$
		Normal Ordering (best fit)		Inverted Ordering ($\Delta\chi^2 = 6.4$)	
		bfp $\pm 1\sigma$	3σ range	bfp $\pm 1\sigma$	3σ range
with SK atmospheric data	$\sin^2\theta_{12}$	$0.303^{+0.012}_{-0.012}$	$0.270 \to 0.341$	$0.303^{+0.012}_{-0.011}$	$0.270 \to 0.341$
	$\theta_{12}/^\circ$	$33.41^{+0.75}_{-0.72}$	$31.31 \to 35.74$	$33.41^{+0.75}_{-0.72}$	$31.31 \to 35.74$
	$\sin^2\theta_{23}$	$0.451^{+0.019}_{-0.016}$	$0.408 \to 0.603$	$0.569^{+0.016}_{-0.021}$	$0.412 \to 0.613$
	$\theta_{23}/^\circ$	$42.2^{+1.1}_{-0.9}$	$39.7 \to 51.0$	$49.0^{+1.0}_{-1.2}$	$39.9 \to 51.5$
	$\sin^2\theta_{13}$	$0.02225^{+0.00056}_{-0.00059}$	$0.02052 \to 0.02398$	$0.02223^{+0.00058}_{-0.00058}$	$0.02048 \to 0.02416$
	$\theta_{13}/^\circ$	$8.58^{+0.11}_{-0.11}$	$8.23 \to 8.91$	$8.57^{+0.11}_{-0.11}$	$8.23 \to 8.94$
	$\delta_{\rm CP}/^\circ$	232^{+36}_{-26}	$144 \to 350$	276^{+22}_{-29}	$194 \to 344$
	$\frac{\Delta m^2_{21}}{10^{-5}\ {\rm eV}^2}$	$7.41^{+0.21}_{-0.20}$	$6.82 \to 8.03$	$7.41^{+0.21}_{-0.20}$	$6.82 \to 8.03$
	$\frac{\Delta m^2_{3\ell}}{10^{-3}\ {\rm eV}^2}$	$+2.507^{+0.026}_{-0.027}$	$+2.427 \to +2.590$	$-2.486^{+0.025}_{-0.028}$	$-2.570 \to -2.406$

Fig. 16: Three-flavor oscillation parameters from the fit to global data as of November 2022. The numbers in the 1st (2nd) column are obtained assuming NO (IO), i.e., they are relative to the respective local minimum.

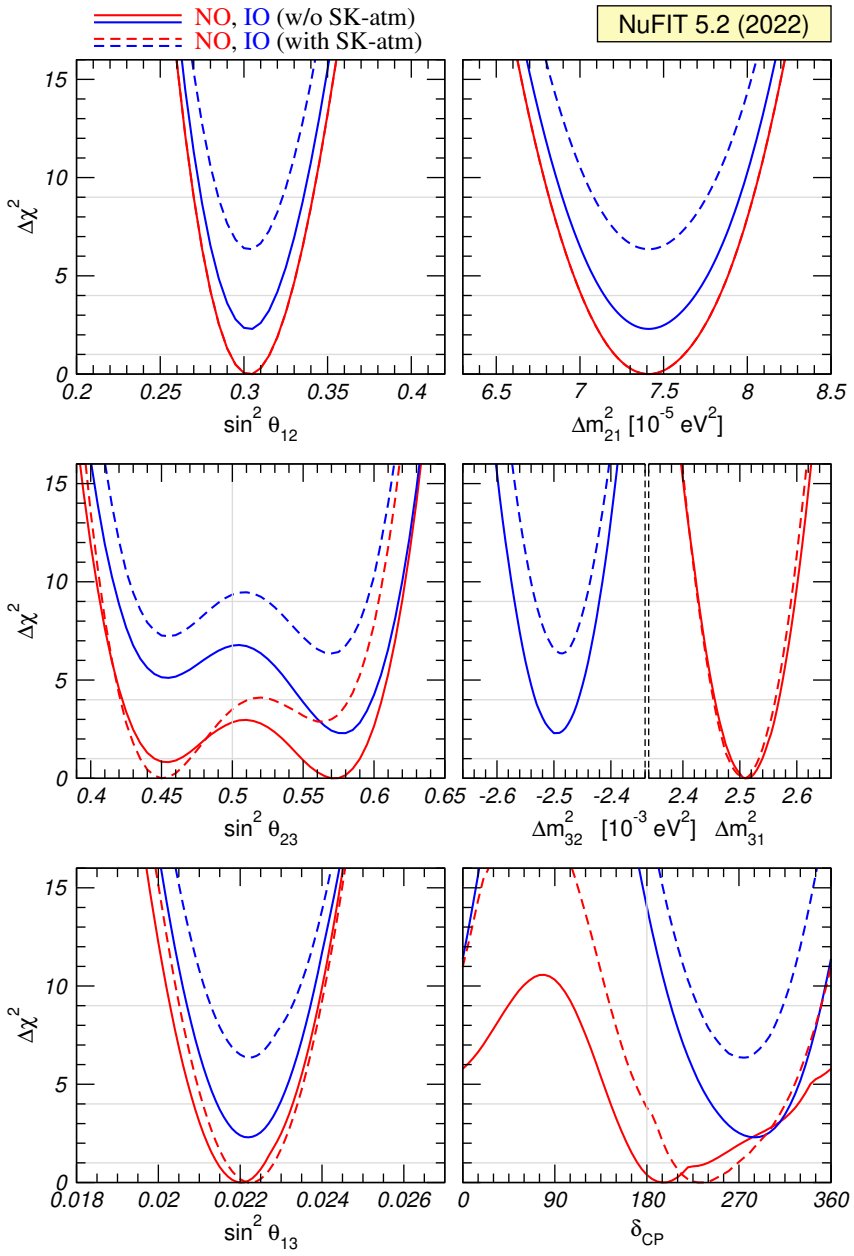

Fig. 17: Resulting χ^2 distributions for the global 3ν oscillation analysis of Fig. 16. The red (blue) curves are for NO (IO). The solid (dashed) lines are obtained without (with) the inclusion of SK-atm χ^2 data.

representations of the two MO possibilities [65]. While recent T2K [66], NOνA [67] and SK [68] experiments report individually that their data favor mildly NO, a study [69] shows no favor in that indication with the combined data from the experiments. This ambiguity in determining the neutrino MO is worthy of further investigation. Measurements of $|\Delta m^2_{31}|$ are carried on in three main chain channels: (i) $\nu_\mu \to \nu_\mu$ (or $\bar{\nu}_\mu \to \bar{\nu}_\mu$) with accelerator-based LBL (A-LBL) neutrino experiments and atmospheric neutrino experiments; (ii) $\nu_\mu \to \nu_e$ (or $\bar{\nu}_\mu \to \bar{\nu}_e$) with A-LBL neutrino experiment; and (iii) $\bar{\nu}_e \to \bar{\nu}_e$ with the reactor-based SBL(R-SBL) neutrino experiments. The probabilities for the two cases, NO and IO, as function of the neutrino energies for the first two channels are shown in Fig. 19.

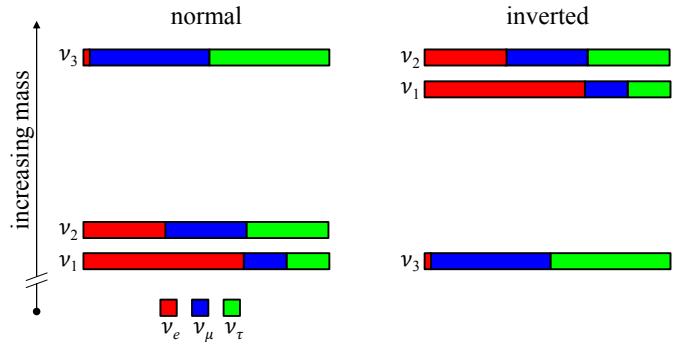

Fig. 18: Pictorial representations of two possible neutrino mass orderings (figure taken from Ref. [64]).

It is deduced from Fig. 19 that the sensitivity to the neutrino MO is marginal in the $\nu_\mu \to \nu_\mu$ (or $\bar{\nu}_\mu \to \bar{\nu}_\mu$) disappearance channels. The effect of the neutrino MO, on the other hand, is much stronger in the $\nu_\mu \to \nu_e$ (or $\bar{\nu}_\mu \to \bar{\nu}_e$) appearance channels. The relatively large modification of the oscillation probabilities in this channel is due to the coherent scattering of electron (anti-) neutrinos on the electrons present in the matter—the MSW effect. However, one must consider the fact that the $\nu_\mu \to \nu_e$ (or $\bar{\nu}_\mu \to \bar{\nu}_e$) appearance probability is just a few percentage, limiting the statistics of the collected data sample. Moreover, extracting the neutrino MO effect from the appearance probabilities is non-trivial since the sign of Δm^2_{31} is tangled severely with $\delta_{\rm CP}$ and the mixing angle θ_{23} (it also depends on the mixing angle θ_{13}, which we know with 3% precision), which have been measured with relatively large uncertainty. In addition, it is important to note that the modifications of the $\nu_\mu \to \nu_e$ and $\bar{\nu}_\mu \to \bar{\nu}_e$ appearance probabilities due to matter effects are not the same.

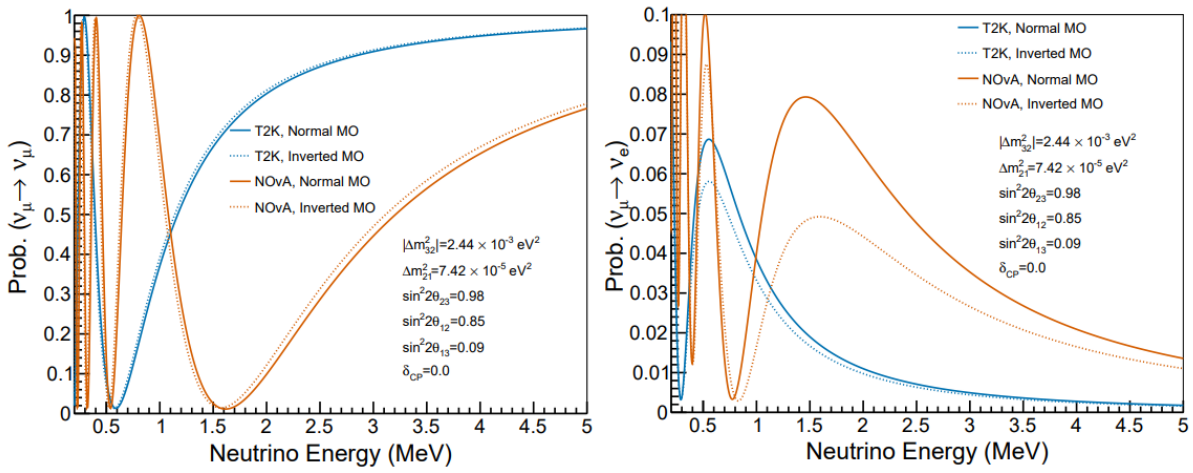

Fig. 19: Neutrino oscillation probabilities for ν_μ (or $\overline{\nu}_\mu$) disappearance (left) and ν_e appearance (right) for the T2K and NOνA experiments with two possible MO hypotheses (figure taken from Ref. [70]).

Due to the mutual dependence of the considered parameters in the neutrino oscillation probabilities, determining the neutrino MO will apparently enhance the sensitivity of the CP-violation search and vice

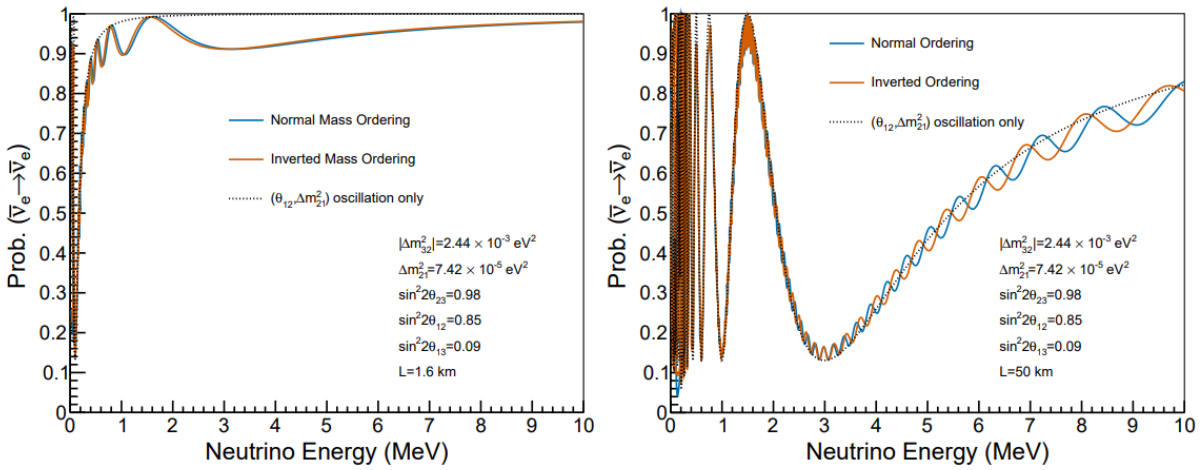

Fig. 20: The $\overline{\nu}_e$ survival probabilities in the reactor-based neutrino experiments with short (left) and medium (right) experimental baselines (figure taken from Ref. [70]).

versa. As a result, the program to elucidate the neutrino MO and the search for CP violation in the A-LBL neutrino experiments are inextricably linked. So far, in the case of the R-SBL neutrino experiments, we have investigated with detectors placed relatively close to the reactor core, a few hundred meters to a few kilometers from the neutrino source. As shown on the left side of Fig. 20, the sensitivity to the neutrino MO is marginal. However, JUNO [58], with a medium-baseline of 50 km, can improve the sensitivity to the neutrino MO thanks to the interference between two oscillation terms [71], which are driven by Δm^2_{21} and Δm^2_{31}, respectively.

For JUNO, the most challenging thing to achieve is an excellent resolution of the reconstructed neutrino energy to unravel the neutrino MO effect from the detector response effect. The recent progress on the JUNO calibration [72] demonstrates that this unprecedented achievement in energy resolution is viable. In addition, it is important to note that, unlike when measuring the neutrino MO with an A-LBL experiment, the sensitivity to the neutrino MO in the reactor-based medium baseline (R-MBL) neutrino experiments is independent of the value of $\delta_{\rm CP}$. Thus, resolving the neutrino MO with A-LBL and R-MBL neutrino experiments is complementary [73].

5.2 Dirac or Majorana masses ?

5.2.1 Dirac masses

For a Dirac field given by $\psi = \begin{pmatrix} \varphi \\ \chi \end{pmatrix}$, we can separate left-handed and right-handed fields by using projection operators, $P_{L(R)}$, as follows:

$$\begin{aligned} \psi_L = P_L\psi = \frac{1}{2}(1-\gamma^5)\psi = \begin{pmatrix} \varphi \\ 0 \end{pmatrix} \ , \\ \psi_R = P_R\psi = \frac{1}{2}(1+\gamma^5)\psi = \begin{pmatrix} 0 \\ \chi \end{pmatrix} \ . \end{aligned} \tag{24}$$

Similarly, $\overline{\psi}_L = \overline{\psi}P_R, \overline{\psi}_R = \overline{\psi}P_L$. Then a Dirac field is composed of two fields ψ_L and ψ_R as $\psi = \psi_L + \psi_R$. The fermion mass term is written as $\overline{\psi}\psi = \overline{\psi}_R\psi_L + \overline{\psi}_L\psi_R$, and the coefficients of the terms correspond to the mass of the fermion ψ. This result shows that a fermion mass can be thought of as a $L \leftrightarrow R$ transition. For an electron (or positron), e_L (or $\bar{e}_R \equiv (e^c)_R$: a short bar (-) on top stands for an antiparticle) is a component of an iso-doublet with $I_3 = -(+)\frac{1}{2}$, whereas $e_R(\bar{e}_L)$ is an iso-singlet. Then, a Dirac mass of electrons (positrons) is constructed by combining both $e_L(\bar{e}_R)$ and $e_R(\bar{e}_L)$. But the combination of $e_L(e_R)$ and $\bar{e}_R(\bar{e}_L)$ is not allowed due to violation of conservation of electric charge. In order to make neutrinos massive, a new degree of freedom with an iso-singlet is required. A very simple possibility is to postulate the existence of new Weyl fermions, N_R, with no SM quantum numbers. They do not affect SM gauge anomaly cancellations and are only modestly constrained by experiments. SM gauge singlet fermions couple to the SM only via neutrino – Higgs boson Yukawa interactions;

$$\mathcal{L}_{\nu Yuk} = y_\nu \overline{L} H N_R \ + \ \text{h.c.} \ , \tag{25}$$

where y_ν is the Yukawa coupling, L is a lepton doublet and H is a SM Higgs. After electroweak symmetry is broken, the left-handed neutrino ν in L and a singlet N_R combine into a massive neutrino with mass $m_D = y_\nu v$, where v is the vacuum expectation value of H, which is called a neutrino Dirac mass. This type of neutrino mass is similar to that of other charged leptons. In order to make the neutrino Dirac mass tiny, of order 0.1 eV, the Yukawa coupling y_ν must be around 10^{-12}. The size of y_ν is very small compared with other Yukawa couplings in the SM. Such a small Yukawa coupling may serve as a hint of new physics beyond the SM. In general, m_D is a $N \times N$ complex matrix when we consider N generation of leptons. Then, m_D is diagonalized by a bi-unitary transformation like $m_D = U M^D V^\dagger$, where U corresponds to the rotation matrix of left-handed neutrinos and V to that of right-handed neutrinos.

5.2.2 Majorana masses

In 1937, Majorana formulated a new theory of neutrinos, whereby the neutrino and the antineutrino are indistinguishable, and suggested the antineutrino-induced β-decay as an experimental verification of this hypothesis [74]. To understand the properties of Majorana neutrinos, let us consider some basic relations. The charge conjugation of the field ψ is defined by

$$\psi^c \equiv \bar{\psi} = C\overline{\psi}^T \ , \qquad C = i\gamma^2\gamma^0 \ , \tag{26}$$

where C is the charge conjugation operator and γ^i is the gamma matrix . Then, the following relations hold:

$$(\psi_R)^c = \bar{\psi}_L \ , \qquad (\psi_L)^c = \bar{\psi}_R \ . \tag{27}$$

Let $\psi_L = \begin{pmatrix} \varphi \\ 0 \end{pmatrix}$, then its charge conjugate becomes $(\psi_L)^c = C\gamma^0\psi_L^* = \begin{pmatrix} 0 \\ -i\sigma^2\varphi^* \end{pmatrix}$. Combining both gives a fermion satisfying the relation $\psi = \bar{\psi}$, which is the condition for a Majorana neutrino. We need

only φ to describe a Majorana neutrino, as follows:

$$\psi_M = \psi_L + (\psi_L)^c = \begin{pmatrix} \varphi \\ -i\sigma^2\varphi^* \end{pmatrix} = \bar{\psi}_M \ . \tag{28}$$

Note that, in the same representation for a Majorana neutrino, a Dirac fermion can be written as $\psi_D = \begin{pmatrix} \varphi \\ -i\sigma^2\chi^* \end{pmatrix}$, $(\varphi \neq \chi)$. Then, if $\varphi = \chi$, it becomes a Majorana fermion. Using Eq. (27), a Majorana fermion can be written as

$$\psi_M = \begin{cases} \psi_L + (\psi_L)^c = \psi_L + \bar{\psi}_R \\ \psi_R + (\psi_R)^c = \psi_R + \bar{\psi}_L \end{cases} . \tag{29}$$

Then, the Majorana mass term becomes

$$\mathcal{L} \ = \ \overline{\psi}_M M \psi_M \ + \ \text{h.c.} \ = \ \overline{\psi}_L M (\psi_L)^c + \overline{\bar{\psi}}_L M \psi_L \ + \ \text{h.c.} \tag{30}$$

Note that the Majorana mass matrix is symmetric, and can therefore be diagonalized by an unitary mixing matrix such as $U^\dagger M U^* = M_{\text{diag}}$. The Majorana mass terms are not invariant under $\psi \to e^{i\alpha}\psi$. So, lepton number is not conserved in the Majorana mass term.

If the nature of the neutrinos is Majorana, then they can be emitted and absorbed in the same process without showing up in the corresponding final state [75]. The neutrinoless double beta decay ($0\nu\beta\beta$), $(A, Z) \to (A, Z+2) + 2e^-$, is a commonly proposed and experimentally pursued theoretical radioactive decay process that would prove a Majorana nature of the neutrinos, as shown in Fig. 21. It would also indicate the first ever signal of non-conservation of total lepton number. The amplitude for the decay rate depends on the effective neutrino mass, defined by $\langle m_{\beta\beta} \rangle = \sum_i U_{ei}^2 m_i$. Experimentally of interest and thus measured is the sum of the kinetic energies of the two emitted electrons. It should equal the total released kinetic energy of the respective nucleus for neutrinoless double beta emission. To search for neutrinoless double beta decay, there are currently a number of experiments underway and several future experiments were proposed for increased sensitivity.

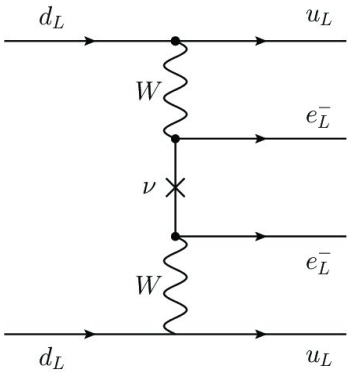

Fig. 21: Feynman diagram for neutrinoless double beta decay due to exchange of light Majorana neutrino ν (figure taken from Ref. [76]).

5.2.3 *Seesaw mechanism*

Once N_R is introduced to make neutrinos massive, as far as the SM is concerned, there is no symmetry to prohibit the mass term, $M\overline{N}_R\bar{N}_L$ where M is the Majorana mass. Then, it is possible to consider the Majorana neutrino $N = N_R + \bar{N}_L$. Putting possible mass terms for neutrinos together, the mass terms can be written in the matrix form as follows:

$$(\overline{\nu_L, \bar{N}_L}) \begin{bmatrix} 0 & m_D \\ m_D^T & M \end{bmatrix} \begin{pmatrix} \bar{\nu}_R \\ N_R \end{pmatrix} . \tag{31}$$

Note that the mass term combining ν_L and $\bar{\nu}_R$ implies $I_3 = 1, Y + -2$ and thus is forbidden by weak isospin. But if a new scalar triplet with $I_3 = 1, Y = 2$ is introduced, the mass term can be generated. Assuming $M \gg m_D$, diagonalization of the mass matrix in (31) leads to two mass eigenvalues of which the lighter one is given by $m_\nu = -m_D M^{-1} m_D^T$. As M gets larger, m_ν gets smaller. Its behavior looks like a seesaw, so we call it a seesaw mechanism [77–83] that successfully makes m_ν tiny when M is large enough. There is no guide to determine the scale of m_D as well as of M. Taking $m_D \sim 100$ GeV, we need $M \sim 10^{15}$ GeV to achieve $m_\nu \sim \sqrt{\Delta m^2_{atm}} \sim 0.05$ eV. Alternatively, there are so-called type-II [84–87] and type-III [88] seesaw models in which a new scalar triplet and a new fermion triplet are introduced, respectively. There are also several models that realize tiny neutrino masses via quantum effects [89,90]. The seesaw mechanisms, as well as the radiative generations of neutrino masses, provide possible answers to why light neutrino masses are so tiny. However, there is no experimental hint for them yet.

5.3 Determination of neutrino mass

As mentioned, we cannot determine the absolute values of neutrino masses through neutrino oscillation experiments. Then, how can we determine them experimentally? One possible way is to use decay kinematics. The simplest case is the 2-body at-rest-decay kinematics of $\pi \to \mu\nu_\mu$, for which one can easily obtain the relation

$$m_\nu^2 = m_\pi^2 + m_\mu^2 - \sqrt{4m_\pi^2(|\vec{p}_\mu|^2 + m_\mu^2)} . \tag{32}$$

Using the relation, we can extract the value of m_ν. However, it is hard to do it with this method, mainly because of uncertainties in measuring m_π, m_μ and $|\vec{p}_\mu|$. Now, the most plausible method is to extract information on the scale of neutrino mass from the endpoint spectrum of the ${}^3\mathrm{H} \to {}^3\mathrm{He}^+ + e^- + \bar{\nu}_e$, beta decay, with energy threshold $E_0 = 18.6$ keV. The idea that the neutrino mass can be deduced in that way was already recognized by Fermi [3] in 1934, when he formulated the theory of beta decay. This method is called a "direct measurement" since it is model independent and does only rely on energy and momentum conservation. The number of events of the tritium beta decay depends on

$$m^2(\nu_e) = \sum |U_{ei}|^2 m^2(\nu_i) . \tag{33}$$

The endpoint spectrum of the beta decay would be shifted along with the value of $m^2(\nu_e)$. But, to observe modification of the endpoint spectrum, we need an eV-scale E resolution, very high luminosity,

very low background and an accurate theoretical prediction of the integral spectrum. There are a few experiments to determine the absolute scale of neutrino mass.

The KATRIN experiment [91] addresses these challenges by combining a high-activity molecular tritium source with a high-resolution spectrometer of the magnetic adiabatic collimation and electrostatic (MAC-E)-filter type16. Recently, KATRIN reported a new upper limit on the neutrino mass of 0.8 eV, by using the Lokhov–Tkachov or Feldman–Cousins technique, which is the first time that a direct neutrino mass experiment has entered the sub-eV mass range [92]. Figure 22 presents the evolution of the best fit $m^2(\nu_e)$ results from various neutrino-mass measurements to date. Compared with other measurements, the result from the KATRIN experiment has narrowed the statistical and systematic uncertainties.

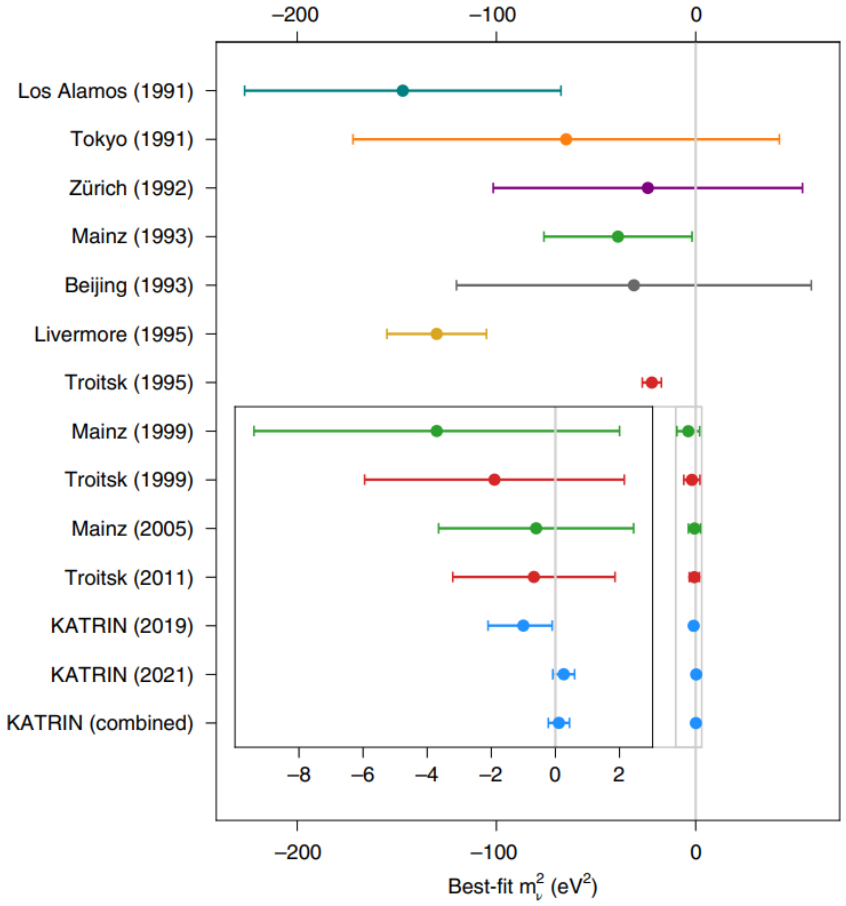

Fig. 22: Evolution of the $m^2(\nu_e)$ best-fit values and total uncertainties from neutrino mass experiments [92].

6 CP violation in neutrino oscillations

Charge conjugation is the transformation associated with the exchange between a particle and an antiparticle, whereas parity changes a left-handed state into a right-handed state, and vice-versa. Under CP transformation, left-handed and right-handed fermion fields become, respectively,

$$(\psi_L)^{\rm CP} = i\sigma^2\psi_L^* \,, \qquad (\psi_R)^{\rm CP} = -i\sigma^2\psi_R^* \,. \tag{34}$$

An important observable concerned with CP symmetry is the so-called Jarlskog invariant defined by $\mathrm{Im}[U^*_{\alpha k}U_{\beta k}U_{\alpha j}U^*_{\beta j}] = \pm J = \pm \hat{J}\sin\delta_{\rm CP}$, with $\hat{J} = c_{12}s_{12}c_{23}s_{23}c^2_{13}s_{13}$ for the lepton sector. Under CP transformation, the mixing element U and J go to U^* and $-J$, respectively. As can be seen from Eq. (10), the oscillation probability is composed of a CP conserving part (second term) and a CP violating part (third term). Since the CP violating part vanishes for $\alpha = \beta$, CP violation can be explored through the appearance channels, $\nu_\alpha \to \nu_\beta$. Under CP transformation, the transition probability $P_{\nu_\alpha\to\nu_\beta}(= P^{\rm CPC}_{\nu_\alpha\to\nu_\beta} + P^{\rm CPV}_{\nu_\alpha\to\nu_\beta})$ goes to $P_{\bar{\nu}_\alpha\to\bar{\nu}_\beta}(= P^{\rm CPC}_{\nu_\alpha\to\nu_\beta} - P^{\rm CPV}_{\nu_\alpha\to\nu_\beta})$. CP violation shows up as a difference between $P_{\nu_\alpha\to\nu_\beta}$ and $P_{\bar{\nu}_\alpha\to\bar{\nu}_\beta}$, which is called the CP asymmetry, $A^{\rm CP}_{\alpha\beta}$, defined by

$$A^{\rm CP}_{\alpha\beta} \equiv \frac{P_{\nu_\alpha\to\nu_\beta} - P_{\bar{\nu}_\alpha\to\bar{\nu}_\beta}}{P_{\nu_\alpha\to\nu_\beta} + P_{\bar{\nu}_\alpha\to\bar{\nu}_\beta}} = \frac{P^{\rm CPV}_{\nu_\alpha\to\nu_\beta}}{P^{\rm CPC}_{\nu_\alpha\to\nu_\beta}} \quad (\alpha \neq \beta)\ . \tag{35}$$

Since the detection of ν_e and ν_μ is far easier than that of ν_τ, the golden channel for CP asymmetry is $A^{\rm CP}_{\mu e}$. To leading order in $\Delta m^2_{21}L/(2E) \equiv \Delta_{21}$, the CP asymmetry $A^{\rm CP}_{\mu e}$ approximately becomes

$$A^{\rm CP}_{\mu e} \simeq \frac{4\sin\Delta_{21}\hat{J}\sin\delta_{\rm CP}}{\sin^2\theta_{23}\sin^2 2\theta_{13}} \simeq \frac{c_{23}\sin 2\theta_{12}}{s_{12}s_{13}}\left(\frac{\Delta m^2_{21}}{\Delta m^2_{31}}\right)\frac{\Delta m^2_{31}L}{4E} \sim 0.26\left(\frac{\Delta m^2_{31}L}{4E}\right)\ . \tag{36}$$

We see from Eq. (36) that the asymmetry grows linearly with L, but for fixed detector size and neutrino energy E, the flux of neutrinos decreases as $\sim 1/L^2$. The first oscillation maximum occurs at

$$L_0 = \frac{2\pi E}{\Delta m^2_{31}} \simeq 495\left(\frac{E}{\rm GeV}\right)\left(\frac{2.5\times10^{-3}}{\Delta m^2_{31}}\right)\ {\rm km}\ . \tag{37}$$

For an example, the detector of the T2K experiment is located at 295 km away from the accelerator, so as to observe the first oscillation maximum for neutrinos with $E \sim 0.6$ GeV. The observation of CP asymmetry is achievable at LBL experiments. Indeed, the measurement of CP violation can become more complicated because of the fact that the oscillation probabilities for neutrinos and anti-neutrinos are in general different in matter even if $\delta_{\rm CP} = 0$. The approximated form of the transition probability in matter is given by Ref. [93]

$$\begin{aligned}
P_{\nu_\alpha\to\nu_\beta} \;\sim\;& \sin^2\theta_{23}\sin^2 2\theta_{13}\sin^2\frac{\Delta_{31}}{2}\left(1 - \frac{8a}{\Delta m^2_{31}}\cos 2\theta_{13}\right) \\
&+ c^2_{13}(c^2_{23}\sin^2 2\theta_{12} + 4s^2_{13}s^2_{23}s^4_{12} - 2s_{13}s^2_{12}\sin 2\theta_{12}\sin 2\theta_{23}\cos\delta)\sin^2\frac{\Delta_{21}}{2} \\
&+ c^2_{13}(s^2_{13}\sin 2\theta_{12}\sin\theta_{23}\cos\delta_{\rm CP} - 4s^2_{23}s^2_{12}s^2_{13})\sin^2\frac{\Delta_{31}}{2}\sin\frac{\Delta_{21}}{2} \\
&+ 8\hat{J}\sin\frac{\Delta_{31}}{2}\sin\frac{\Delta_{21}}{2}\sin\frac{\Delta_{32}}{2}\sin\delta_{\rm CP} \\
&+ 2\cos 2\theta_{13}\sin^2 2\theta_{13}s^2_{23}\left(\frac{aL}{4E}\right)\sin\frac{\Delta_{31}}{2}\cos\frac{\Delta_{32}}{2}\ ,
\end{aligned} \tag{38}$$

where $a[{\rm eV}^2] = 2\sqrt{2}G_F N_e E = 7.6\times10^{-3}\rho[{\rm g/cm}^3]\,E[{\rm GeV}]$ stands for the matter effect. G_F, N_e and ρ represent the Fermi constant, number density of electron and matter density of Earth, respectively. Under CP transformation, a goes to $-a$, which mimics CP violation.

Figure 23 shows how $P_{\nu_\mu\to\nu_e}$ and $P_{\bar{\nu}_\mu\to\bar{\nu}_e}$ differently evolve over E for fixed $\delta_{\rm CP}$ and L. The left

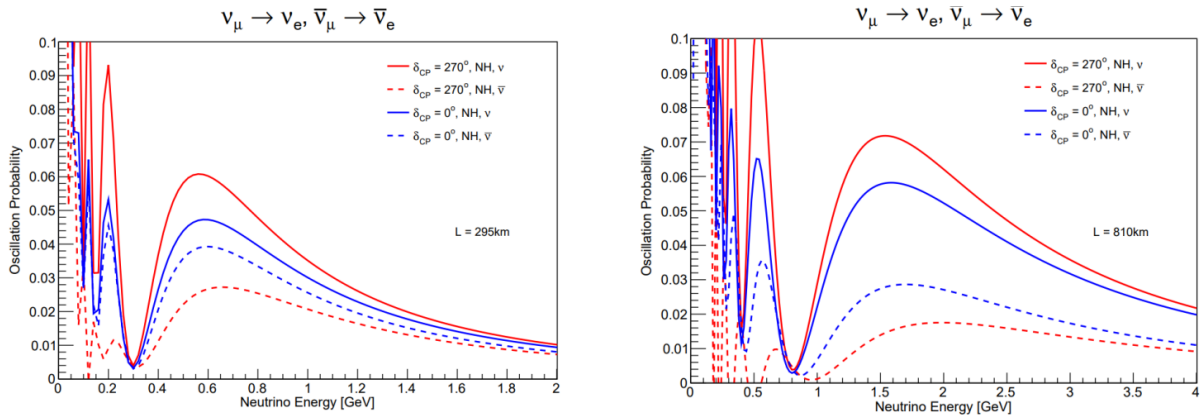

Fig. 23: Transition probabilities $P_{\nu_\mu \to \nu_e}$ and $P_{\overline{\nu}_\mu \to \overline{\nu}_e}$ as functions of neutrino energy for T2K baseline L = 295 km (a) and NOνA baseline L = 810 km (b) [94].

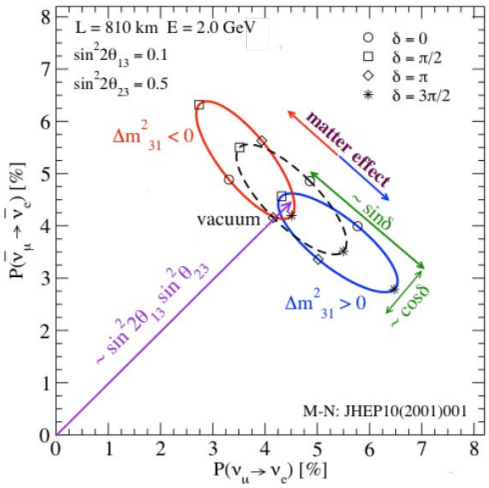

Fig. 24: Bi-probability diagram in the space $P_{\nu_\mu \to \nu_e}$ *vs.* $P_{\overline{\nu}_\mu \to \overline{\nu}_e}$ for the NOνA experiment.

(right) panel corresponds to the T2K (NOνA) baseline. The solid (dashed) lines correspond to the neutrino (anti-neutrino) oscillation, and the red (blue) curves to $\delta_{\rm CP} = 270°(0°)$. Figure 24 presents a CP trajectory diagram in bi-probability space as a powerful tool for a pictorial representation of the genuine CP and matter effects in neutrino oscillations [95]. If we vary $\delta_{\rm CP}$ from 0 to 2π, we can draw a closed trajectory, which becomes an ellipse, in the $P - \bar{P}$ plane. How far the ellipse is away from the origin is proportional to $\sin^2\theta_{13}$. For $\delta_{\rm CP} = 0$ or π, there is no difference between the two probabilities. Taking into account matter effects, the ellipse is shifted to two different directions according to the sign of Δm^2_{31}, i.e. matter effects for $(+)\Delta m^2_{31}$ enhance P, whereas for $(-)$ they suppress P. The magnitude of shift is larger as the matter effects, as well as the baseline, are larger. If the distance is short, the two trajectories may overlap. The octant of θ_{23} can be distinguished using this diagram. Figure 25 shows

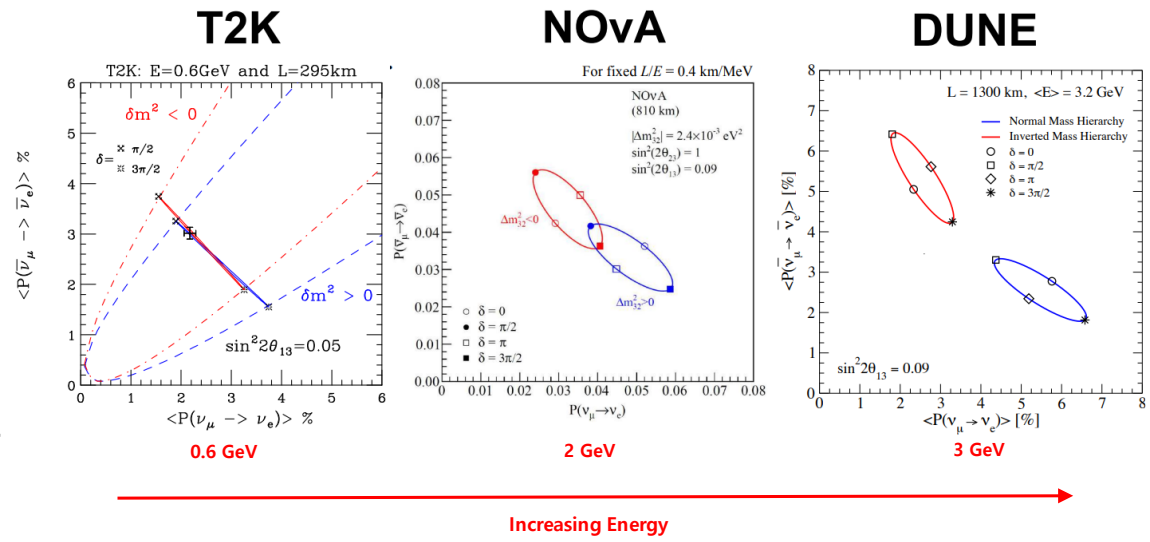

Fig. 25: Comparison of bi-probabilities for the T2K, NoνA and DUNE experiments (figure taken from Ref. [96]).

how the neutrino MO and CP violation can be disentangled for experiments with different L and E. As expected, the chance to disentangle them would be increased as E and L get larger. There are some implications on CP violation in the lepton sector coming from the results of NOνA [97] and T2K [98] experiments. Figure 26 shows the favored regions of the parameter space $(\delta_{\rm CP}, \sin^2\theta_{23})$. The upper (lower) panel corresponds to NO (IO). The colored regions are results obtained from NOνA, whereas the regions surrounded by black contours are from T2K. We see that both results for IO are consistent, whereas there is a tension between them for NO at 2 σ level. The NOνA and T2K experiments will continue to take data till 2026 and 2027, respectively, and then the statistics of present analyses are expected to be double. The future experiments such as DUNE and Hyper-Kamiokande will achieve the sensitivities to determine whether CP is violated in the lepton sector or not.

7 Conclusion

In the past few decades, a very important breakthrough in particle physics was made by the discovery of neutrino oscillations, which has shown neutrino properties beyond the SM. In this lecture, a full understanding of the various aspects of the neutrino oscillations was provided. The various experiments studying neutrinos from different sources were discussed, ranging from the pioneering ones to the experiments still in operation and to those in preparation. I have shown how the parameters concerned with neutrino oscillations were investigated and determined from the experiments. The most important milestones and the results of neutrino experiments were presented. The origin of neutrino masses and the principle behind the observed leptonic structure have been addressed. I have presented various attempts to identify the nature of neutrinos, establish the absolute values of neutrino masses, determine their or-

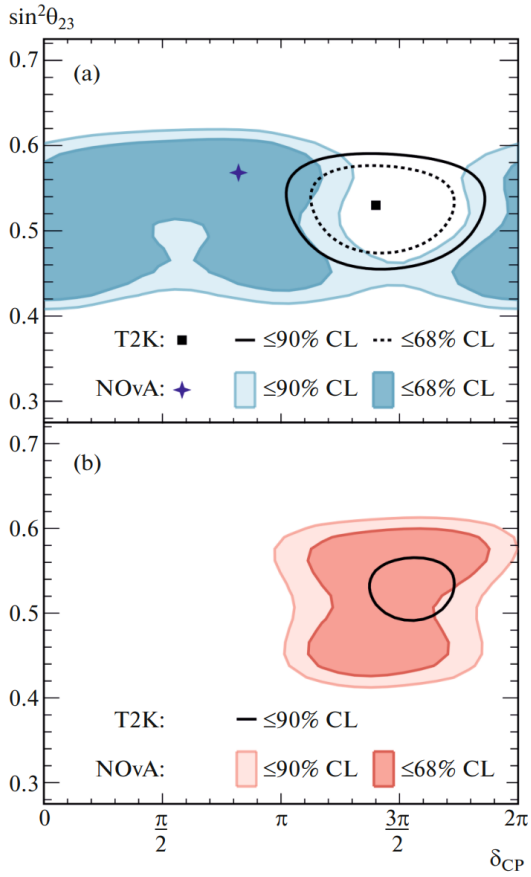

Fig. 26: Allowed regions of ($\delta_{\rm CP}$, $\sin^2\theta_{23}$) from the T2K (black contours) and NOνA (colored regions) experiments [97, 98]. The upper (lower) plot corresponds to NO (IO).

dering, and measure the CP violating phase. Despite being challenging, exciting experimental programs are underway and planned for the future and will be able to address the unsolved issues.

Acknowledgement

I sincerely thank the students and the organizers of the 2022 Asia–Europe–Pacific School of High-Energy Physics for the amazing success of the school. I was supported by the National Research Foundation of Korea (NRF) grants NRF-2019R1A2C1088953 and NRF-2020K1A3A7A09080135.

References

[1] Y. Fukuda *et al.* [Super-Kamiokande] *Phys. Rev. Lett.* **81** (1998) 1562–1567, doi:10.1103/PhysRevLett.81.1562.

[2] J. Chadwick, *Proc. Royal Soc. A* **136** (1932) 692–708, doi:10.1098/rspa.1932.0112.

[3] E. Fermi, *Z. Phys.* **88** (1934) 161–177, doi:10.1007/BF01351864.

[4] A. Pais, *Inward bound of matter and forces in the physical world* (Oxford Univ. Press, Oxford, 1986) p. 418.

[5] C.L. Cowan *et al.*, *Sci.* **124** (1956) 103–104, doi:10.1126/science.124.3212.103.

[6] G. Danby *et al.*, *Phys. Rev. Lett.* **9** (1962) 36–44, doi:10.1103/PhysRevLett.9.36.

[7] M.L. Perl *et al.*, *Phys. Rev. Lett.* **35** (1975) 1489–1492, doi:10.1103/PhysRevLett.35.1489.

[8] J. Jackson *et al.*, Press release: Physicists find first direct evidence for tau neutrino at Fermilab (Fermilab, Batavia, IL, 20 Jul. 2000); K. Kodama *et al.* [DONUT], *Phys. Lett. B* **504** (2001) 218–224, doi:10.1016/S0370-2693(01)00307-0.

[9] G. Barbiellini *et al.*, Neutrino counting, Proc. Workshop on Z Physics at LEP1, CERN, Switzerland, edited by G. Altarelli, R.H.P. Kleiss and C. Verzegnassi, CERN-89-08, vol. 1 (CERN, Geneva, 1989), pp. 129–170, doi:10.5170/CERN-1989-008-V-1.129;
D. Decamp *et al.* [ALEPH], *Phys. Lett. B* **231** (1989) 519–529, doi:10.1016/0370-2693(89)90704-1;
P. Aarnio *et al.* [DELPHI], *Phys. Lett. B* **231** (1989) 539–547, doi:10.1016/0370-2693(89)90706-5;
B. Adeva *et al.* [L3], *Phys. Lett. B* **231** (1989) 509–518, doi:10.1016/0370-2693(89)90703-X;
M.Z. Akrawy *et al.* [OPAL], *Phys. Lett. B* **231** (1989) 530–538, doi:10.1016/0370-2693(89)90705-3.

[10] S. Eidelman *et al.*, *Phys. Lett. B* **592** (2004) 1, doi:10.1016/j.physletb.2004.06.001; `http://pdg.lbl.gov`.

[11] B. Pontecorvo, *Zh. Eksp. Teor. Fiz.* **33** (1958) 549–551; *Sov. Phys. JETP* **6** (1957) 429–431, https://inspirehep.net/literature/2884.

[12] Z. Maki, M. Nakagawa and S. Sakata, *Prog. Theor. Phys.* **28** (1962) 870–880, doi:10.1143/PTP.28.870.

[13] B. Pontecorvo, *Zh. Eksp. Teor. Fiz.* **53** (1967) 1717–1725; *Sov. Phys. JETP* **26** (1968) 984–988, https://inspirehep.net/literature/51319.

[14] R. Davis, Jr., D.S. Harmer and K.C. Hoffman, *Phys. Rev. Lett.* **20** (1968) 1205–1209, doi:10.1103/PhysRevLett.20.1205.

[15] V.N. Gribov and B. Pontecorvo, *Phys. Lett. B* **28** (1969) 493–496, doi:10.1016/0370-2693(69)90525-5.

[16] Q.R. Ahmad *et al.* [SNO], *Phys. Rev. Lett.* **87** (2001) 071301, doi:10.1103/PhysRevLett.87.071301.

[17] D. Casper *et al.*, *Phys. Rev. Lett.* **66** (1991) 2561–2564, doi:10.1103/PhysRevLett.66.2561.

[18] K.S. Hirata *et al.* [Kamiokande-II], *Phys. Lett. B* **205** (1998) 416–420, doi:10.1016/0370-2693(88)91690-5.

[19] M. Hirsch, The quest for neutrino mass, lecture at the 4th Chilean School of High Energy Physics, 13–15 Jan. 2016, Indico.

[20] L. Wolfenstein, *Phys. Rev. D* **17** (1978) 2369–2374, doi:10.1103/PhysRevD.17.2369.

[21] S.P. Mikheyev and A.Y. Smirnov, *Sov. J. Nucl. Phys.* **42** (1985) 913.

[22] S.J. Parke, *Phys. Rev. Lett.* **57** (1986) 1275–1278, doi:10.1103/PhysRevLett.57.1275.

[23] T.K. Gaisser and M. Honda, *Ann. Rev. Nucl. Part. Sci.* **52** (2002) 153–199, doi:10.1146/annurev.nucl.52.050102.090645.

[24] W.W.M. Allison *et al.*, *Phys. Lett. B* **391** (1997) 491–500, doi:10.1016/S0370-2693(96)01609-7.

[25] Y. Fukuda *et al.* [Kamiokande], *Phys. Lett. B* **335** (1994) 237–245, doi:10.1016/0370-2693(94)91420-6.

[26] T. Kajita and P. Lipari, "*Comptes Rendus Physique* **6** (2005) 739–748, doi:10.1016/j.crhy.2005.07.004.

[27] T. Kajita *et al.* [Super-Kamiokande], *Nucl. Phys. B* **908** (2016) 14–29, doi:10.1016/j.nuclphysb.2016.04.017.

[28] P. Adamson *et al.*, *Nucl. Instrum. Meth. A* **806** (2016) 279–306, doi:10.1016/j.nima.2015.08.063.

[29] D. Beavis *et al.* [E899], Long Baseline Neutrino Oscillation Experiment: Physics design report, BNL 52459 (Brookhaven National Lab., Upton, NY, 1995), doi:10.2172/52878.

[30] Y. Hayato *et al.* [T2K] Letter of intent: Neutrino Oscillation Experiment at JHF (2003), https://inspirehep.net/literature/640246.

[31] K. Abe *et al.* [T2K], *Phys. Rev. Lett.* **107** (2011) 041801, doi:10.1103/PhysRevLett.107.041801.

[32] K. Abe *et al.* [T2K], *Phys. Rev. D* **87** (2013) 012001, doi:10.1103/PhysRevD.87.012001.

[33] D. Michael, *Nucl. Phys. B Proc. Suppl.* **118** (2003) 189–196, doi:10.1016/S0920-5632(03)01317-3.

[34] P. Adamson *et al.* [MINOS], *Phys. Rev. Lett.* **110** (2013) 251801, doi:10.1103/PhysRevLett.110.251801.

[35] G. Tzanankos *et al.* [MINOS+], MINOS+: a Proposal to FNAL to run MINOS with the medium energy NuMI beam, FERMILAB-PROPOSAL-1016 (2011), https://inspirehep.net/literature/944685

[36] A. Habig [NOvA], *Nucl. Phys. B Proc. Suppl.* **229–232** (2012) 460, doi:10.1016/j.nuclphysbps.2012.09.097.

[37] M.A. Acero *et al.* [NOvA], *Phys. Rev. Lett.* **123** (2019) 151803, doi:10.1103/PhysRevLett.123.151803.

[38] L. Berns [T2K], [arXiv:2105.06732 [hep-ex]], 10.48550/arXiv.2105.06732.

[39] J.N. Bahcall, *Neutrino astrophysics* (Cambridge Univ. Press, 1989).

[40] J.N. Bahcall, *Phys. Rev. Lett.* **12** (1964) 300–302, doi:10.1103/PhysRevLett.12.300.

[41] R. Davis, *Phys. Rev. Lett.* **12** (1964) 303–305, doi:10.1103/PhysRevLett.12.303.

[42] W. Hampel *et al.* [GALLEX], *Phys. Lett. B* **447** (1999) 127–133, doi:10.1016/S0370-2693(98)01579-2.

[43] J.N. Abdurashitov *et al.* [SAGE], *Phys. Rev. C* **60** (1999) 055801, doi:10.1103/PhysRevC.60.055801.

[44] Y. Fukuda *et al.* [Super-Kamiokande], *Phys. Rev. Lett.* **81** (1998) 1158–1162, doi:10.1103/PhysRevLett.81.1158, [Erratum-ibid. **81** (1998) 4279, doi:10.1103/PhysRevLett.81.4279].

[45] J. Boger *et al.* [SNO], *Nucl. Instrum. Meth. A* **449** (2000) 172–207, doi:10.1016/S0168-9002(99)01469-2.

[46] B. Aharmim *et al.* [SNO], *Phys. Rev. C* **75** (2007) 045502, doi:10.1103/PhysRevC.75.045502.

[47] Q.R. Ahmad *et al.* [SNO], *Phys. Rev. Lett.* **89** (2002) 011301, doi:10.1103/PhysRevLett.89.011301.

[48] A. Bellerive *et al.* [SNO], *Nucl. Phys. B* **908** (2016) 30–51, doi:10.1016/j.nuclphysb.2016.04.035.

[49] J.N. Bahcall, M.H. Pinsonneault and S. Basu, *Astrophys. J.* **555** (2001) 990–1012, doi:10.1086/321493.

[50] G. Bellini *et al.*, *Phys. Rev. Lett.* **107** (2011) 141302, doi:10.1103/PhysRevLett.107.141302.

[51] G. Bellini, *Nucl. Phys. B* **908** (2016) 178–198, doi:10.1016/j.nuclphysb.2016.04.011.

[52] K. Eguchi *et al.* [KamLAND], *Phys. Rev. Lett.* **90** (2003) 021802, doi:10.1103/PhysRevLett.90.021802.

[53] S. Abe *et al.* [KamLAND], *Phys. Rev. Lett.* **100** (2008) 221803, doi:10.1103/PhysRevLett.100.221803.

[54] Y. Nakajima, Recent results and future prospects from Super-Kamiokande, talk given at XXIX Int. Conf. on Neutrino Physics and Astrophysics, 22 Jun. –2 Jul. 2020, doi:10.5281/zenodo.4134680.

[55] F. Ardellier *et al.* [Double Chooz], [arXiv:hep-ex/0606025 [hep-ex]], doi:10.48550/arXiv.hep-ex/0606025.

[56] J.K. Ahn *et al.* [RENO], [arXiv:1003.1391 [hep-ex]], doi:10.48550/arXiv.1003.1391.

[57] X. Guo *et al.* [Daya Bay], [arXiv:hep-ex/0701029 [hep-ex]], doi:10.48550/arXiv.hep-ex/0701029.

[58] Z. Djurcic *et al.* [JUNO], [arXiv:1508.07166 [physics.ins-det]], doi:10.48550/arXiv.1508.07166.

[59] F.P. An *et al.* [Daya Bay], *Phys. Rev. Lett.* **108** (2012) 171803, doi:10.1103/PhysRevLett.108.171803.

[60] J.K. Ahn *et al.* [RENO], *Phys. Rev. Lett.* **108** (2012) 191802, doi:10.1103/PhysRevLett.108.191802.

[61] Y. Abe *et al.* [Double Chooz], *Phys. Rev. D* **86** (2012) 052008, doi:10.1103/PhysRevD.86.052008.

[62] The results in Figs. 16 and 17 are taken from `http:www.nu-fit.org`.

[63] E. Di Valentino and A. Melchiorri, *Astrophys. J. Lett.* **931** (2022) L18, doi:10.3847/2041-8213/ac6ef5.

[64] R. B. Patterson, *Ann. Rev. Nucl. Part. Sci.* **65** (2015) 177, doi:10.1146/annurev-nucl-102014-021916.

[65] P. Fernández, *SciPost Phys. Proc.* **1** (2019) 029, doi:10.21468/SciPostPhysProc.1.029.

[66] J. Lagoda [T2K], *PoS* **NuFact2021** (2022) 054, doi:10.22323/1.402.0054.

[67] E. Catano-Mur [NOvA], [arXiv:2206.03542 [hep-ex]], doi:10.48550/arXiv.2206.03542.

[68] P. Fernandez Menendez [Super-Kamiokande], *PoS* **ICRC2021** (2021) 008, doi:10.22323/1.395.0008.

[69] K.J. Kelly *et al.*, *Phys. Rev. D* **103** (2021) 013004, doi:10.1103/PhysRevD.103.013004.

[70] S. Cao *et al.*, *Symmetry* **14** (2022) 1, doi:10.3390/sym14010056.

[71] S.T. Petcov and M. Piai, *Phys. Lett. B* **533** (2002) 94–106, doi:10.1016/S0370-2693(02)01591-5.

[72] A. Abusleme *et al.* [JUNO], *JHEP* **03** (2021) 004, doi:10.1007/JHEP03(2021)004.

[73] S. Cao *et al.*, *Phys. Rev. D* **103** (2021) 112010, doi:10.1103/PhysRevD.103.112010.

[74] E. Majorana, *Nuovo Cim.* **14** (1937) 171–184, doi:10.1007/BF02961314.

[75] W. Rodejohann, *Int. J. Mod. Phys. E* **20** (2011) 1833–1930, doi:10.1142/S0218301311020186.

[76] J.J. Gomez-Cadenas *et al.*, *Riv. Nuovo Cim.* **35** (2012) no.2, 29–98, doi:10.1393/ncr/i2012-10074-9.

[77] H. Fritzsch, M. Gell-Mann and P. Minkowski, *Phys. Lett. B* **59** (1975) 256–260, doi:10.1016/0370-2693(75)90040-4.

[78] P. Minkowski, *Phys. Lett. B* **67** (1977) 421–428, doi:10.1016/0370-2693(77)90435-X.

[79] T. Yanagida, *Prog. Theor. Phys.* **64** (1980) 1103–1105, doi:10.1143/PTP.64.1103.

[80] M. Gell-Mann, P. Ramond and R. Slansky, Proc. Supergravity Workshop, Stony Brook, NY, United States, 27–28 Sep. 1979, edited by D.Z. Freedman and P.van Nieuwenhuizen (North-Holland, Amsterdam, 1979), pp. 315-321, https://inspirehep.net/literature/9686.

[81] S.L. Glashow, The future of elementary particle physics, Proc. Cargese Summer Institute: Quarks and leptons, edited by M. Lévy *et al.* (Plenum, New York, NY, 1980), pp. 687–713, doi:10.1007/978-1-4684-7197-7_15.

[82] R. N. Mohapatra and G. Senjanovic, *Phys. Rev. Lett.* **44** (1980) 912, doi:10.1103/PhysRevLett.44.912.

[83] J. Schechter and J.W.F. Valle, *Phys. Rev. D* **22** (1980) 2227, doi:10.1103/PhysRevD.22.2227.

[84] M. Magg and C. Wetterich, *Phys. Lett. B* **94** (1980) 61–64, doi:10.1016/0370-2693(80)90825-4.

[85] T.P. Cheng and L.F. Li, *Phys. Rev. D* **22** (1980) 2860, doi:10.1103/PhysRevD.22.2860.

[86] G. Lazarides, Q. Shafi and C. Wetterich, *Nucl. Phys. B* **181** (1981) 287–300, doi:10.1016/0550-3213(81)90354-0.

[87] R.N. Mohapatra and G. Senjanovic, *Phys. Rev. D* **23** (1981) 165, doi:10.1103/PhysRevD.23.165.

[88] R. Foot *et al.*, *Z. Phys. C* **44** (1989) 441, doi:10.1007/BF01415558.

[89] A. Zee, *Phys. Lett. B* **93**, 389 (1980), doi:10.1016/0370-2693(80)90349-4, [Erratum-ibid. **95**, 461 (1980), doi:10.1016/0370-2693(80)90193-8].

[90] Y. Cai textitet al., *Front. in Phys.* **5** (2017) 63, doi:10.3389/fphy.2017.00063.

[91] A. Osipowicz *et al.* [KATRIN], [arXiv:hep-ex/0109033 [hep-ex]], doi:10.48550/arXiv.hep-ex/0109033.

[92] M. Aker *et al.* [KATRIN], *Nature Phys.* **18** (2022) 160, doi:10.1038/s41567-021-01463-1.

[93] H. Nunokawa, S.J. Parke and J.W.F. Valle, *Prog. Part. Nucl. Phys.* **60** (2008) 338–402, doi:10.1016/j.ppnp.2007.10.001.

[94] T. van Ngoc, C.V. Son and N.T.H. Van, *Commun. Phys.* **28** (2018) 337, doi:10.15625/0868-3166/28/4/12930.

[95] H. Minakata and H. Nunokawa, *JHEP* **10** (2001) 001, doi:10.1088/1126-6708/2001/10/001.

[96] J. Hartnell, Status and prospects of neutrino mass hierarchy and CP-violation measurements, talk given at Symmetries in Subatomic Physics, Aachen, 11 Jun. 2018, Indico.

[97] A. Himmel, New oscillation results from the NOνA experiment, talk given at XXIX Int. Conf. on Neutrino Physics and Astrophysics, 22 Jun. –2 Jul. 2020, doi:10.5281/zenodo.4142045.

[98] P. Dunne, Latest neutrino oscillations from T2K, talk given at XXIX Int. Conf. on Neutrino Physics and Astrophysics, 22 Jun. –2 Jul. 2020, https://doi.org/10.5281/zenodo.4154355.